Geologic and geodetic constraints on the magnitude and frequency of earthquakes along Malawi's active faults: The Malawi Seismogenic Source Model (MSSM)

Jack N. Williams[1,2*], Luke N. J. Wedmore[1], Åke Fagereng[2], Maximilian J. Werner[1], Hassan Mdala[3], Donna J Shillington[4], Christopher A Scholz[5], Folarin Kolawole[6], Lachlan J. M. Wright[5], Juliet Biggs[1], Zuze Dulanya[7], Felix Mphepo[3], Patrick Chindandali[8]

[1]School of Earth Sciences, University of Bristol, Bristol, UK
[2]School of Environmental Sciences, Cardiff University, Cardiff, UK
[3]Geological Survey Department, Mzuzu Regional Office, Mzuzu, Malawi
[4]School of Earth and Sustainability, Northern Arizona University, Flagstaff, Arizona, USA
[5]Department of Earth and Environmental Sciences, Syracuse University, Syracuse, New York, USA
[6]BP America, Houston, Texas, U.S.
[7]Geography and Earth Sciences Department, University of Malawi, Zomba, Malawi
[8]Geological Survey Department, Zomba, Malawi

*now at the Department of Geology, University of Otago, Dunedin, New Zealand

Correspondence to: Jack N. Williams (jack.williams@otago.ac.nz)

Abstract. Active fault data are commonly used in seismic hazard assessments, but there are challenges in deriving the slip rate, geometry, and frequency of earthquakes along active faults. Herein, we present the open-access geospatial Malawi Seismogenic Source Model (MSSM, https://doi.org/10.5281/zenodo.6779638), which describes the seismogenic properties of faults that have formed during ongoing East African rifting in Malawi. We first use empirically derived constraints to geometrically classify active faults into section, fault, and multi-fault seismogenic sources. For sources in the North Basin of Lake Malawi, slip rates can be derived from the vertical offset of a seismic reflector that is estimated to be 75 ka based on dated core. Elsewhere, slip rates are constrained from advancing a 'systems-based' approach that partitions geodetically-derived rift extension rates in Malawi between seismogenic sources using a priori constraints on regional strain distribution in magma-poor continental rifts. Slip rates are then combined with source geometry and empirical scaling relationships to estimate earthquake magnitudes and recurrence intervals, and their uncertainty is described from the variability of outcomes from a logic tree used in these calculations. Sources in the MSSM are 5-200 km long, which implies that large magnitude (M_W 7-8) earthquakes may occur in Malawi. However, low slip rates (0.05-2 mm/yr) mean that the frequency of such events will be low (recurrence intervals ~10^3-10^4 years). We also find that for 9 out of 11 faults in Lake Malawi's North Basin, differences in the slip rates, when estimated independently from the geodetic data and the offset seismic reflector, are not statistically

significant. The MSSM represents an important resource for investigating Malawi's increasing seismic risk and provides a framework for incorporating active fault data into seismic hazard assessment elsewhere in the East African Rift and other tectonically active regions.

1. Introduction

Earthquake hazards are most frequently quantified as the probability of exceeding a specific ground motion intensity in a given time period through probabilistic seismic hazard analysis (PSHA; e.g., Cornell, 1968; Gerstenberger et al., 2020; McGuire, 1995). The main components of a PSHA are seismogenic sources, which cumulatively describe the magnitude and frequency of earthquakes within the assessed region, and a ground motion model, which describes the ground motion intensities earthquakes will induce. Typically, seismogenic sources are developed from using the historical and instrumental records of earthquakes to develop areal or smoothed seismicity models (e.g., Goitom et al., 2017; Helmstetter and Werner, 2012; Poggi et al., 2017), and/or combining geologic, paleoseismic, and/or geodetic information to describe the magnitude and frequency of earthquakes on known active faults through fault-based seismogenic sources (e.g., Gómez-Novell et al., 2020; Morell et al., 2020; Pace et al., 2016; Pagani et al., 2020; Stirling et al., 2012). However, there remain many challenges and uncertainties in for when incorporating these data into PSHA (e.g., Morell et al., 2020).

For example, an estimate of the earthquake recurrence interval and/or slip rate is required to assess earthquake frequency on active faults (e.g., Molnar, 1979; Wallace, 1970; Youngs and Coppersmith, 1985). Typically, slip rates are derived from: (1) planar or linear geologic features that have been offset by a fault and have a known age (McCalpin, 2009) and/or (2) geodetic measurements of surface interseismic strain accumulation using Global Navigation Satellite Systems, and from which fault slip rates are constrained using 1D velocity profiles (Bendick et al., 2000), 2D block models (Wallace et al., 2012; Zeng and Shen, 2014), or by partitioning regional geodetically measured strain across multiple faults (Cox et al., 2012; Williams et al., 2021a). However, whilst geodetic measurements have been made only over the past few decades, offset geologic markers sample the displacement accrued by a fault over timescales of 10^2-10^5 years. This is problematic as earthquakes along a single fault may temporally cluster (Cowie et al., 2012; DuRoss et al., 2020; Wedmore et al., 2017; Weldon et al., 2004), and/or there may be transient variations in the rate of interseismic strain accumulation (Dolan and Meade, 2017; Hetland and Hager, 2006). In either case, this implies that a fault's slip rate will not necessarily be the same when measured at different temporal scales (Beauval et al., 2018; Bormann et al., 2016; Cowie and Roberts, 2001; Fagereng and Biggs, 2019; Litchfield et al., 2014; Petersen et al., 2014; Polonia et al., 2004).

The likely magnitude of an earthquake along an active fault can be inferred from empirically-derived scaling relationships between fault geometry (e.g. length or area) and magnitude (Kanamori and Anderson, 1975; Leonard, 2010; Stirling et al., 2013; Thingbaijam et al., 2017; Wells and Coppersmith, 1994; Wesnousky, 2008). However, faults do not necessarily rupture along their full length in a single event but may also host shorter ruptures bound by along-strike geometrical complexities,

65   and/or longer 'multi-fault' earthquakes where adjacent faults rupture simultaneously (Biasi and Wesnousky, 2016, 2017; DuRoss et al., 2016; Fletcher et al., 2014; Litchfield et al., 2018). Furthermore, large magnitude (M>~7) earthquakes can extend across the full width of the crust's seismogenic layer, and in these cases, it is unclear how fault area scales with magnitude (Hanks and Bakun, 2002; Leonard, 2010; Shaw, 2013; Shaw and Scholz, 2001). The regional strain rate and tectonic environment from which empirical earthquake scaling data are collated will also influence these relationships (Stirling et al.,
70   2013).

Cumulatively, these challenges mean there is aleatory variability (i.e., the uncertainty related to the stochastic nature of earthquake occurrence) and epistemic uncertainty (i.e., the uncertainty related to limited datasets or knowledge of the earthquake process) when developing fault-based seismogenic sources (Gerstenberger et al., 2020; Marzocchi et al., 2015;
75   Morell et al., 2020). Hence, despite its intuitive premise, questions remains about the extent to which geological fault information improves the skill of probabilistic earthquake forecasts at the timescales (50-1,000 years) of interest in PSHA (Nicol et al., 2016; Rhoades et al., 2018; Strader et al., 2017; Taroni et al., 2018; Zechar et al., 2013). More pertinently, many regions currently lack the active fault data required to develop fault-based seismogenic sources (Perea et al., 2006; Styron and Pagani, 2020; Williams et al., 2021a).

80

In this study, we present the Malawi Seismogenic Source Database (MSSM), in which we collate estimates for the geometry, slip rate, and earthquake magnitude, and recurrence interval of faults included in the Malawi Active Fault Database (Williams et al., 2022b), and whose development has required addressing many of the challenges described above. For example, fault slip rates have been previously derived in central and northern Malawi based on the offset of a 75 ka reflector in seismic
85   reflection surveys in Lake Malawi (Shillington et al., 2020) whilst in southern Malawi, slip rates have been inferred by partitioning geodetically-derived regional extension rates across faults (Williams et al., 2021a). By extending the use of geodetic methods to estimate fault slip rates in Lake Malawi, we can use the MSSM to test whether slip rates derived at timescales from 10^1 to 10^5 years in Malawi can be reconciled. Furthermore, we outline how the observed along-strike segmentation of active faults in Malawi (Accardo et al., 2018; Contreras et al., 2000; Hodge et al., 2018a, 2019; Laõ-Dávila
90   et al., 2015; Macheyeki et al., 2015; Scholz et al., 2020; Shillington et al., 2020; Wedmore et al., 2020b, 2020a), fault intersections at depth (Gaherty et al., 2019; Scholz and Contreras, 1998), and a 30-40 km thick seismogenic layer (Craig and Jackson, 2021; Ebinger et al., 2019; Nyblade and Langston, 1995; Stevens et al., 2021) are incorporated into the MSSM earthquake magnitude estimates. Previous estimates of earthquake recurrence intervals in southern Malawi were constrained only between 10^2-10^5 years (Williams et al., 2021a). However, in the MSSM we incorporate a new geodetic model that has
95   smaller uncertainties (Wedmore et al., 2021), and we describe a new probabilistic approach to more rigorously describe recurrence interval and slip rate uncertainties.

Cumulatively, the steps taken to investigate fault geometry, slip rate, and earthquake source properties in the MSSM will be of interest to other regional seismic hazard studies, particularly those with few geologic and geodetic constraints on fault activity. Seismic risk in Malawi, and elsewhere along the East African Rift, is increasing because of rapid population growth and the proliferation of seismically vulnerable building stock (Delvaux et al., 2017; Giordano et al., 2021; Goda et al., 2016, 2021; Hodge et al., 2015; Ngoma et al., 2019; Novelli et al., 2019). The geospatial, kinematic, and earthquake source data in the MSSM are freely available, and we suggest that the database will be an important resource for seismic hazard planning in the region.

2. Seismotectonic setting of Malawi

2.1 Tectonic setting of Malawi

A ~900-km-long section of the East African Rift's (EAR) Western Branch passes through Malawi (Fig. 1). Geodetic models imply that this section of the EAR accommodates 0.5-1.5 mm/yr ENE-WSW extension between the San and Rovuma plates (Fig. 1; Wedmore et al., 2021). In central and northern Malawi, the EAR has been flooded by Lake Malawi, whilst in southern Malawi, the rift floor and associated faults are subaerially exposed (Fig. 1b). South of the Rungwe Volcanic Province in southwestern Tanzania, there is no reported surface volcanism and only minor, if any, melts in the lower crust (Accardo et al., 2020; Hopper et al., 2020; Njinju et al., 2019; Wang et al., 2019). The Malawi section of the EAR is therefore considered to be magma-poor.

A multidisciplinary dataset of 113 fault traces was compiled by Williams et al., (2021b, 2022b) in the Malawi Active Fault Database (MAFD). The MAFD includes 90 basement-involved faults that were mapped from geological maps, high resolution digital elevation models, and 2D seismic reflection surveys (Scholz et al., 2020; Shillington et al., 2020; Williams et al., 2019; Wedmore et al., 2020) and that have demonstrably shown evidence of displacement during EAR activity in Malawi. The remaining 23 faults in the MAFD are buried intrarift faults inferred from aeromagnetic (Kolawole et al., 2018a, 2021a) or gravity data (Chisenga et al., 2019). These faults therefore exhibit no definitive evidence of displacements associated with East African rifting, but they are well-oriented for reactivation in the regional stress field (Dawson et al., 2018; Williams et al., 2019, 2022b). The MAFD contains basic geomorphic and mapping attributes following the format of the Global Earthquake Model Global Active Faults Database (Styron and Pagani, 2020). In keeping with practice elsewhere (Faure Walker et al., 2021; Styron et al., 2020) the MSSM contains data that are considered to be more subjective and may be liable to change (e.g. earthquake recurrence intervals).

2.2 Seismicity in Malawi

The instrumental record of seismicity in Malawi is complete for events $M_W > 4.5$ from 1965 (Fig. 1; Hodge et al., 2015; Poggi et al., 2017). In this record, the largest event in Malawi is the 1989 M_W 6.3 Salima Earthquake with its unusually deep focal

depth (32 ± 5 km) demonstrative of the region's thick seismogenic layer (Fig. 1b; Jackson and Blenkinsop, 1993). Recent local deployments of seismometers in northern and southern Malawi demonstrate that the base of this seismogenic layer is
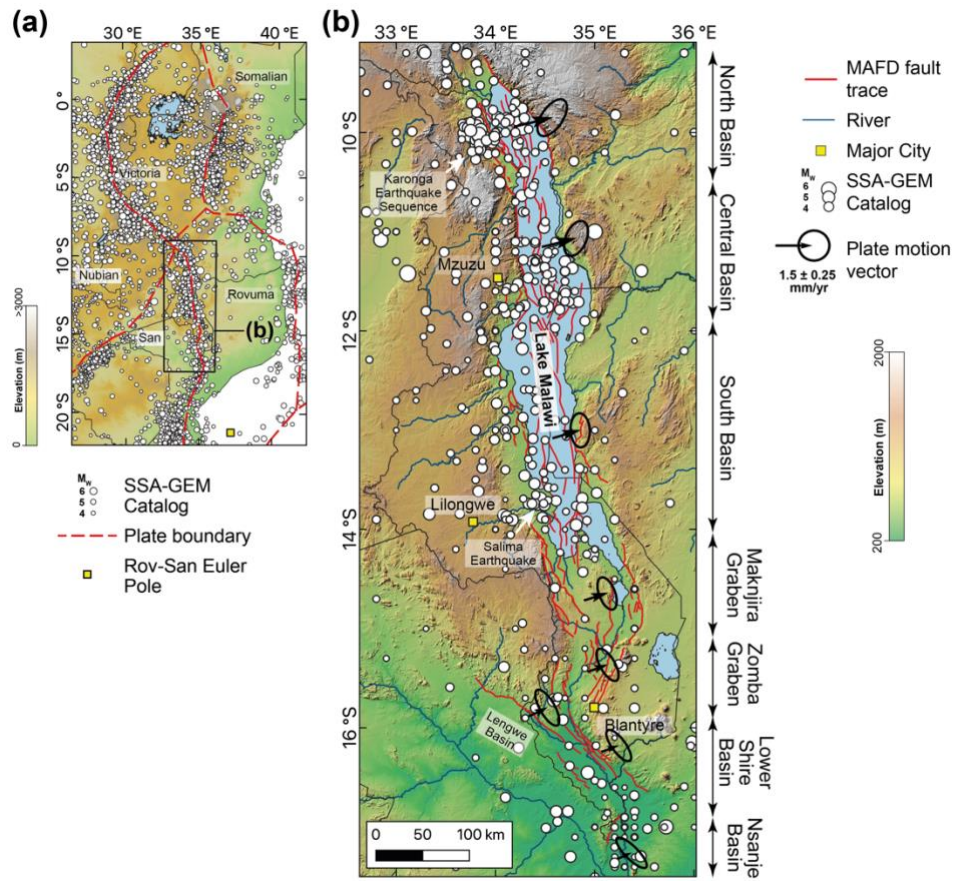
Figure 1: (a) Location of Malawi within the context of an East African Rift scale geodetic model (Wedmore et al., 2021) and earthquake locations from the Sub-Saharan Africa Global Earthquake Model Catalog (SSA-GEM; Poggi et al., 2017). (b) The Malawi Active Fault Database (MAFD) and major EAR basins in Malawi (Williams et al., 2022b). Plate motion vector for central point of each basin for the Rovuma-San Euler pole (Wedmore et al., 2021), with error ellipse modelled using methods described in Robertson et al., (2016). Figures underlain by (a) 90 m resolution Global 30 Arc-Second Elevation (GTOPO30) Digital Elevation Model and (b) Shuttle Radar Topography Mission 30 m DEM (Sandwell et al., 2011).

approximately coincident with the Moho (35-45 km; Ebinger et al., 2019; Njinju et al., 2019; Stevens et al., 2021; Sun et al., 2021; Wang et al., 2019), however, the data cannot resolve whether the two coincide, if there is an interval of aseismic lower crust, or if seismicity extends into the upper lithospheric mantle. In either case, earthquakes may nucleate throughout the seismogenic layer (Ebinger et al., 2019; Stevens et al., 2021) with evidence for moderate-magnitude, shallow seismicity

illustrated by the 2009 Karonga earthquake sequence in northern Malawi (Biggs et al., 2010; Fagereng, 2013). This sequence consisted of four M_W 5.5-5.9 events with focal depths <8 km (Fig. 1b; Biggs et al., 2010; Gaherty et al., 2019) and resulted in a 9- to 18 km-long surface rupture along the previously unrecognised St Mary fault (Hamiel et al., 2012; Kolawole et al., 2018b; Macheyeki et al., 2015). Focal mechanism stress inversions indicate a normal fault stress state in Malawi with an ENE-WSW trending minimum principal compressive stress (σ_3; Delvaux and Barth, 2010; Ebinger et al., 2019; Williams et al., 2019).

Although no M_W>6.5 events have been recorded instrumentally in Malawi, steep 10- to 20-m-high and 50- to 130-km-long fault scarps in Malawi imply that M_W 6.5-7.8 events have occurred in the Late Quaternary (Hodge et al., 2019, 2020; Jackson and Blenkinsop, 1997; Wedmore et al., 2020b, 2020a; Williams et al., 2021a). Furthermore, events of this magnitude have been recorded elsewhere in the EAR Western Branch (Ambraseys, 1991; Ambraseys and Adams, 1991; Ayele and Kulhanek, 2000; Delvaux and Barth, 2010; Fenton and Bommer, 2006; Kervyn et al., 2006; Vittori et al., 1997).

Using the instrumental record of seismicity, PSHA indicates there is a 10 % probability of exceeding (PoE) ~0.15 g in 50 years in Malawi (Poggi et al., 2017). However, when geodetic and geologic data were combined to develop seven fault-based seismogenic sources around Lake Malawi, hazard levels around the fault sources were much higher (10% PoE 0.25 g in 50 years), particularly at low probabilities of exceedance and long vibration periods (Hodge et al., 2015). Scenario-based seismic risk assessment indicates that a full M_W 7.7 rupture of the Bilila-Mtakataka fault in southern Malawi would result in 160,000-440,000 collapsed buildings (Goda et al., 2021).

3. The Malawi Seismogenic Source Model

The Malawi Seismogenic Source Model (MSSM) is a geospatial database that documents the geometry, slip rate, and seismogenic properties (i.e., earthquake magnitude and frequency) of active faults in Malawi (Fig. 2, Table 1). Each geospatial feature represents a potential earthquake rupture or 'source' and is classified based on its geometry into one of three types: section, fault, or multi-fault. Source types are mutually exclusive, and so if incorporated into a PSHA, they should be assigned relative weightings. The MSSM is comparable to the South California Earthquake Centre Community Fault Model (Plesch et al., 2007), Database of Individual Seismogenic Sources in Italy (Basili et al., 2008), the Taiwan Earthquake Model (Shyu et al., 2016), or the New Zealand Community Fault Model (Seebeck et al., 2022). The MSSM is the first seismogenic source database in central and northern Malawi, and represents an update of the South Malawi Seismogenic Source Database (SMSSD; Williams et al., 2021b) because it incorporates newly identified fault traces (Kolawole et al., 2021a; Williams et al., 2022b), new geodetic data (Wedmore et al., 2021) and a new exploration of uncertainty in the logic tree approach (Sect. 3.4).

The MSSM itself consists of two components: (1) a 3D geometrical model of seismogenic sources in Malawi, and (2) a GIS file that comprises a simplified 2D representation of each source, and its source attributes (Table 1). These are freely available

180   **Table 1:** List and brief description of fault geometry, slip rate estimates, and earthquake source attributes in the MSSM. Attributes are assigned to each rupture source, with section, fault, and multi-fault ruptures stored in distinct shapefiles.

Attribute	Type	Description	Notes
MSSM_id	integer	Unique numerical reference ID for each seismic source	ID 00-300 is section rupture ID 300-500 is fault rupture ID 600-700 is a multi-fault rupture
name	string		Assigned based on previous mapping or local geographic feature. For sections and faults, the name of the fault (flt_name) and larger multifault (mflt_name) system they are hosted on are also given respectively.
basin	string	Basin that source is located within.	Used in slip rate calculations (Sect. 3.2).
class	string	Intrarift or border	
length (L_s)	real number	Straight-line distance in km between tips, or sum of L_{sec} for segmented faults, and sum of L_{fault} for multi faults	Measured in km to 1 decimal place. Except for linking sections, must be >5 km (Sect. 3.1.1).
area	integer	Calculated from L_s multiplied by Eq. 1 or based on fault truncation	Measured in km^2.
strike	integer	Measured from tips, using bearing that is <180°.	Input for slip rate estimates (Eq. 2).
dip_lower	integer	Lower range of dip value	When no previous measurements of dip are available, a nominal value of 45° is assigned.

dip_int	integer	Intermediate dip value	In the MSSM geometrical model, only the intermediate measurement is considered. When no previous measurements are available, a nominal value of 53° is assigned. No dip assigned for multi-fault sources, as different participating faults may have different dips.
dip_upper	integer	Upper range of dip value	When no previous measurements of dip are available, a nominal value of 65° is assigned.
dip_dir	string	Compass quadrant that fault dips in.	No dip direction assigned for multi-fault sources, as different participating faults may have different dips.
slip_type	string	Source kinematics	All sources in the MSSM assumed to be normal (Williams et al., 2019).
slip_rate	real number	Mean value from repeating Eq. (2) in Monte Carlo simulations.	In mm/yr. All sources in the MSSM assumed to be normal, so is equivalent to dip-slip rate. Reported to two significant figures
s_rate_err	real number	1σ error from Monte Carlo slip rate simulations.	
mag_lower	real number	Lower magnitude estimate. Calculated from Leonard, (2010) scaling relationship (Eq. 4) for L_s or A_s, and using lower estimates of c_1 and c_2 constants.	Reported to one decimal place
mag_int	real number	Mean magnitude estimate. Calculated from Leonard, (2010) scaling relationship (Eq. 4) for L_s or A_s, and using mean estimates of c_1 and c_2 constants.	Reported to one decimal place
mag_upper	real number	Upper magnitude estimate. Calculated from Leonard, (2010) scaling relationship (Eq. 4) for L_s or A_s, and using upper estimates of c_1 and c_2 constants.	Reported to one decimal place

ri_lower	integer	Calculated as 1σ below the mean value of the Monte Carlo simulations (assuming a log normal distribution).	Reported to two significant figures.
ri_int	integer	Mean value from log of recurrence interval Monte Carlo simulations.	Reported to two significant figures.
ri_upper	integer	Calculated as 1σ above the mean value of the Monte Carlo simulations (assuming a log normal distribution).	Reported to two significant figures.
MAFD_id	integer	ID of equivalent structure in Malawi Active Fault Database (Williams et al., 2022b)	Multifault sources will have multiple ID's.

3.1 MSSM source geometry

3.1.1 MSSM Source Length

For each fault trace in the MAFD, we first assess whether it may host shorter discrete along-strike section ruptures, participate in multi-fault ruptures, and/or exhibit a branching geometry. 'Section' sources in the MSSM are bounded by displacement minima along fault strike, or a >20º bend in fault strike at a scale >5 km (Fig. 2), as these features may be indicative of barriers to dip-slip lateral rupture propagation (Biasi and Wesnousky, 2017; Wedmore et al., 2020b, 2020a). Geometrical complexities that are <5 km long (e.g., relay zone-breaching structures) are interpreted to be 'hard-linking' sections (Peacock et al., 2016), and the insignificant length means they are not considered as distinct sources in the MSSM.

'Fault' seismogenic sources are those that are bounded by the fault tips mapped in the MAFD (Fig. 2). In their compilation of dip-slip surface ruptures, Biasi and Wesnousky, (2017) noted only 10% of earthquakes exhibited branching 'Y' geometries in map view, and the paucity of branching earthquakes is consistent with numerical modelling (Bhat et al., 2007; Geist and Parsons, 2020). Therefore, where we identify fault branches, we consider these as distinct, partially overlapping fault seismogenic sources (Fig. 2).
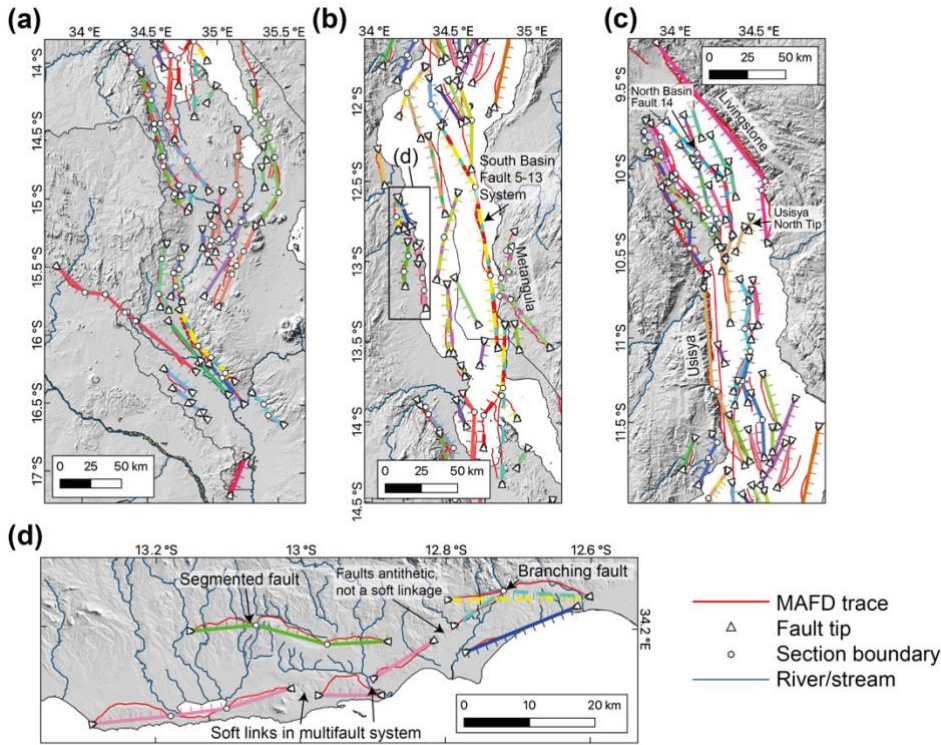
Figure 2: Maps for (a) southern Malawi, (b) South Basin, and (c) Central and North Basins of Lake Malawi showing the simplified geometry of faults in the Malawi Seismogenic Source Database (MSSM). (d) Criteria used to define MSSM sources in central Malawi. The MSSM sources are connected by straight lines between fault tips (triangles) or section boundaries (circles), and colored by each multi-fault or fault system. Ticks indicate dip direction. Dashed or multi-colored sources indicate branching geometries. Thin red lines are the MAFD fault traces (Williams et al., 2022b), and they highlight instances where a MAFD fault is not included in the MSSM, or there is a discrepancy between the MAFD and simplified fault geometry in the MSSM.

'Multi-fault' seismogenic sources are identified in the MSSM where the tips of synthetic faults are closely spaced across-strike, as this may indicate that these faults interact through soft linkages via Coulomb stress changes (Biasi and Wesnousky, 2016; Hodge et al., 2018b; Mildon et al., 2016). Evidence for this behaviour in Malawi is indicated by the bell-shaped along-strike displacement profiles of en-echelon faults in Lake Malawi (Contreras et al., 2000; Mortimer et al., 2016; Shillington et al., 2016). Empirical observations and Coulomb stress modelling indicate that en-echelon synthetic normal faults interact when the across-strike distance between two faults is <20% of the combined length of the faults, up to a maximum separation of 10 km (Biasi and Wesnousky, 2016; Hodge et al., 2018b) and we use this to determine whether two or more distinct faults in the MSSM could rupture together (Fig. 2). Slip on a fault that is close to an across-strike antithetic fault exerts a negative Coulomb

stress change on the antithetic fault (Mildon et al., 2016), and so these cases are not considered as multi-fault sources in the MSSM (Fig. 2d).

215

For fault sources, source length (L_s) is the straight-line distance between fault tips (for unsegmented faults), or the cumulative straight-line distance between the individual section boundaries for segmented faults (Table 1; Fig. 2). Multi-fault source length is the sum of the length of each participating fault (Table 1). Following Christophersen et al., (2015) the minimum length of a MSSM source is 5 km. These length estimates imply shorter lengths than a fault's mapped trace in the MAFD.

220 However, the use of simplified source geometries in the MSSM is consistent with other seismogenic source databases (Basili et al., 2008; Faure Walker et al., 2021; Seebeck et al., 2022), and with the hypothesis that complex surface fault traces in Malawi root onto sub-planar deep-seated (depths > 5 km) weaknesses (Hodge et al., 2018a; Wedmore et al., 2020b). Should a MSSM user want to consider alternative fault source geometries using the MAFD, this database is also readily available (Williams et al., 2021b). However, since other attributes in the MSSM (e.g., magnitude, recurrence interval) are contingent on

225 the source geometries we define, other interpretations of source geometry will require that these attributes are also revised. In instances when accurate fault traces are required (e.g., assessment of surface rupture hazards), the MAFD should be used in preference to the MSSM, as in these cases, the MSSM's simplified geometries will not be realistic.

3.1.2 MSSM Source Width

230 We define the MSSM source geometry as 2D planes in 3D space by projecting the fault sources down-dip, and, in the case of faults in Lake Malawi that were mapped from the offset of the synrift basement surface (Scholz et al 2020), up-dip to the top of the sedimentary package (Figs. 3 and A1). The dip angles of the Livingstone, Chingale Step, Bilila-Mtakataka, Karonga, Kaporo and St Mary faults have been measured directly through either field measurements, geophysical surveys, or microseismicity (Gaherty et al., 2019; Kolawole et al., 2018a; Stevens et al., 2021; Wedmore et al., 2020a; Wheeler and

235 Rosendahl, 1994) and these are applied when projecting faults down-dip. The moderately-steeply dipping (40-65º) planar faults indicated by these studies are also used to bound the dip for MSSM sources where no direct dip measurements are currently available (Table 1), and this uncertainty is incorporated into the slip rate calculations (Sect. 3.2). However, this uncertainty is not incorporated into the MSSM geometrical model, which considers only an intermediate dip estimate of 53º for these sources. The dips and kinematics of linking sections in Malawi have not been directly measured, however, they show

240 distinct dip-slip scarps, and do not coincide with along-strike minima in scarp height or footwall relief (Wedmore et al., 2020b). These linking sections are therefore interpreted as dip-slip planes that dip at the same angle as the adjoining sections, rather than vertically dipping strike-slip sections (Acocella et al., 1999).

Width (W) in the MSSM represents the width of an earthquake a source may host. For relatively short section sources, W will

245 therefore be less than the width of the larger fault or multi-fault structure they are contained within in the MSSM geometrical model (Fig. 3). In practice, this implies that section ruptures can float at a range of depth intervals on a larger fault plane

(Pagani et al., 2014), and so do not necessarily propagate to the surface; indeed, the possible blind rupture of a northern section of the Bilila-Mtakataka Fault during the M_W 6.3 1989 Salima Earthquake may be an example of such an event (Hodge et al., 2018a; Stevens et al., 2021).

250
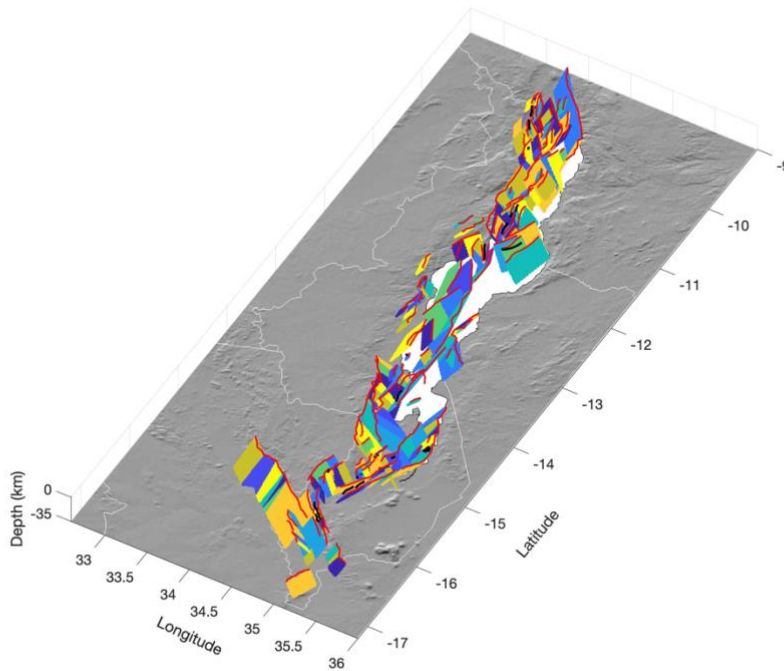
Figure 3: 3D geometrical model of all MSSM sources. Each 2D plane represents a distinct along-strike MSSM section or fault. Red and black lines are the fault traces from the Malawi Active Fault Database (MAFD) that are, and are not, included in the MSSM, respectively. Image underlain by SRTM DEM.

255   In the first instance, W is assigned based on an empirically-derived scaling relation between W and L_s (Leonard, 2010), which are self-consistent with earthquake magnitude and average single event displacement estimates (Sect. 3.3). For dip-slip faults, Leonard, (2010) relations assume that W is unlimited by the thickness of the seismogenic layer. In central and northern Malawi however, faults and multi-fault systems may reach lengths >140 km, which assuming fault dips of ~50-60°, would imply ruptures at depths >40 km. This would be deeper than the 30-40 km thick seismogenic layer in Malawi (Ebinger et al., 2019;
260   Stevens et al., 2021) and would imply that ruptures propagate into the upper mantle. However, our preferred interpretation is that ruptures along faults in the MSSM will not exceed depths of 30-40 km since: (1) mechanically, it is easier for dip-slip ruptures to propagate up-dip rather than down-dip (Das and Scholz, 1983) and (2) estimates of fault width in earthquake scaling relationships are derived from aftershock distributions, and for dip-slip faults, these events do not generally nucleate below the portion of the crust that is seismogenic (Henry and Das, 2001). In the MSSM, W is therefore calculated as:

$$W = \begin{cases} c_1 L_s^{2/3}, & if \ c_1 L_s^{2/3} < \frac{z}{\sin \delta} \\ \frac{z}{\sin \delta}, & if \ c_1 L_s^{2/3} \geq \frac{z}{\sin \delta} \end{cases} \qquad (1)$$

where c_1 is an empirically derived parameter (for interplate dip-slip faults >5 km long; Leonard, 2010), δ is fault dip (53º, unless otherwise measured), and z is the thickness of the seismogenic layer, for which we use an intermediate estimate of 35 km.

270

Following these first estimates for W, we then test whether the down-dip extent of a MSSM source implies that it will intersect with another source at depth (Fig. A1). In this way, we accommodate observations from Malawi and elsewhere that such dip intersections can pose significant barriers to earthquake rupture and/or one of the intersecting faults is truncated by the intersection (Gaherty et al., 2019; King, 1986; Plesch et al., 2007; Walters et al., 2018). In the case where two 2D planes in the MSSM intersect at depth, we assume that the shorter -and presumably lower displacement- source has been truncated and locked by the longer source (Fig. A1; Scholz and Contreras, 1998). Furthermore, if the across-strike distance at the surface between two intersecting sources is <6 km, which is the maximum across-strike distance that two sources dipping at 53º and with widths <5 km will intersect, we omit the shorter of the two sources in the MSSM. In these cases, the slip rate assigned to the simplified MSSM source represents the cumulative slip rate of the main fault strand and its smaller splays.

280

Following the removal of across-strike splays and sources <5 km long (Sect. 3.3.1), 22 faults in the MAFD are not included in the MSSM (Fig. 3, Table S1). This does not imply that these structures cannot host earthquakes but instead that: (1) there are few historical observations of surface ruptures <5 km long (Baize et al., 2019), and this increases the uncertainty in applying earthquake scaling relationships to these faults (Christophersen et al., 2015; Stirling et al., 2013), and (2) there are many hitherto unmapped short (<10 km) faults in Malawi (Williams et al., 2022b), and so during PSHA, it may be more appropriate that moderate magnitude seismicity along them is incorporated using off-fault distributed sources (e.g., Hodge et al., 2015; Stirling et al., 2012).

3.2 Slip Rates

For the MSSM sources in the North Basin of Lake Malawi, slip rates are derived from estimates that were previously made using the vertical offset of a 75 ka megadrought horizon in seismic reflection data (Scholz et al., 2007; Shillington et al., 2020). The offset-reflector slip rate estimates are preferred in the MSSM instead of the geodetic-based estimates (described below), as: (1) they represent on-fault measurements and (2) they represent the slip accumulated over multiple earthquake cycles, and so are more representative of a source's long-term behaviour (Cowie and Roberts, 2001; DuRoss et al., 2020). The uncertainty in using the offset seismic reflector to derive slip rates is discussed in Sect. 3.4.

295

Slip rates are derived from geodesy using a 'systems-based' approach that partitions the regional geodetic extension rate onto rift faults in a manner consistent with observations and theory of regional strain distribution in narrow magma-poor continental rifts (Williams et al., 2021a). We first group the MSSM sources in and adjacent to Lake Malawi into the North, South, and Central Basins (Scholz et al., 2020; Shillington et al., 2020), and in southern Malawi into the Makanjira, Zomba, Lengwe (previously referred to as the "Mwanza"), Lower Shire, and Nsanje basins (Fig. 1b; Williams et al., 2021a). We then divide the MSSM sources based on whether they are part of an intrarift or border fault system. Border faults are classified geometrically in the MSSM as the faults at the edge of the rift (Ebinger, 1989; Muirhead et al., 2019; Williams et al., 2021a). The slip rate for each MSSM source, s, is then estimated through:

$$slip\ rate\ (s) = \begin{cases} \frac{v\alpha_{bf}cos(\theta_s-\phi)}{n_{bf}cos\delta}, & for\ border\ fault\ sources \\ \frac{v\alpha_{if}c_{hwf}cos(\theta_s-\phi)}{n_{if}cos\delta}, & for\ intrarift\ sources \end{cases} \qquad (2)$$

where θ_s is the source's slip azimuth, v and φ are the geodetically-derived horizontal rift extension rate and azimuth, c_{hwf} is a correction factor for hanging-wall flexural extension, α is a weight that depends on whether the source is hosted on a border (α_{bf}) or intrarift (α_{if}) fault system, and it is divided by the number of mapped border (n_{bf}) or intrarift (n_{if}) fault or multi-fault systems in each basin. Uncertainty in these parameters is discussed in Sect. 3.4.

In the MSSM, the rift extension rate (v) and azimuth (φ) are derived from the geodetic model developed by Wedmore et al., (2021) in which southern Africa is divided into two microplates (San and Rovuma) that move independently of the Nubian Plate (Fig. 1). The Euler Pole for the relative motion between San and Rovuma (as defined by a location and rotation rate) and associated uncertainties are used to calculate the plate motion and its uncertainty at the centre of each basin following the methods of Robertson et al (2016) (Table 2, Fig. 1). The MSSM sources are assumed to exhibit pure normal dip-slip, which is consistent with fault slickensides and focal mechanisms (Delvaux and Barth, 2010; Hodge et al., 2015; Wedmore et al., 2020a; Williams et al., 2019), and so the slip azimuth (θ) is parallel to the source's dip direction.

Table 2: Plate motion vector for each basin in Malawi using the geodetic model by Wedmore et al., (2021) and the coordinates from which it was derived. The uncertainties associated with each vector are derived using the methods presented by Robertson et al., (2016). For basins in southern Malawi, the Nubia-Rovuma plate motion vectors obtained from the Saria et al., (2013) geodetic model (S13) and used in the South Malawi Seismogenic Source Database are also reported.

Basin	Centre of basin longitude (E)	Centre of basin latitude (S)	Geodetic Model	Velocity and uncertainty of plate motion (mm/yr)	Azimuth, and azimuthal uncertainty of plate motion

North Basin	34.18	9.93	W21	1.28 ± 0.38	076° ± 016°
Central Basin	34.46	11.16	W21	1.11 ± 0.30	076° ± 017°
South Basin	34.57	13.09	W21	0.91 ± 0.22	074° ± 022°
Makanjira	34.88	14.52	W21	0.75 ± 0.18	073° ± 027°
			S13	1.08 ± 1.66	075° ± 089°
Zomba	34.93	15.43	W21	0.66 ± 0.17	071° ± 032°
			S13	0.88 ± 1.65	072° ± 110°
Lower Shire	35.08	16.23	W21	0.57 ± 0.18	070° ± 037°
			S13	0.69 ± 1.65	069° ± 141°
Nsanje	35.23	17.28	W21	0.57 ± 0.21	067° ± 048°
			S13	0.46 ± 1.63	063° ± 212°
Lengwe	34.33	-15.88	W21	0.61 ± 0.16	065° ± 037°

325 Lower, intermediate, and upper α_{bf} values of 0.5, 0.7, and 0.9 are applied in the MSSM. These values reflect observations of the relative contribution to rift opening between intrarift and border faults in Malawi (Shillington et al., 2020; Wedmore et al., 2020a), elsewhere along the EAR (Kolawole et al., 2021b; Muirhead et al., 2016, 2019; Wright et al., 2020), and in analogue and numerical models (Agostini et al., 2011; Gupta et al., 1998). The South Basin is bound onshore to the east by the Metangula Fault, which exhibits a 500-700 m high escarpment (Laõ-Dávila et al., 2015). However, Flannery and Rosendahl, (1990) have

330 previously interpreted that the South Basin 5-13 multi-fault system, which lies 5-20 km across strike under Lake Malawi (Fig. 2b), is also a border fault given its relatively large length-scale (>200 km) and high throw (>~2 km, as derived from variations in the thickness of synrift sediments across it; Scholz et al., 2020). We consider that the Metangula Fault and South Basin 5-13 multi-fault system represent a pair of border faults that bound the South Basin to the east, and in the MSSM distribute α_{bf} equally between them.

335

The considerable throw (>5 km) along border fault systems in central and northern Malawi induces a significant amount of downward flexure within the rift floor, which is accommodated by intrarift faults (Muirhead et al., 2016; Olive et al., 2014; Petit and Ebinger, 2000). Thus, when considering the slip rate of intrarift sources, the contribution from both regional extensional strain and local flexural strain must be considered. The latter, however, is not sampled by far-field geodetic

340 measurements (Muirhead et al., 2016; Shillington et al., 2020). In Eq. 2, we therefore apply a correction factor (c_{hwf}) to account

for the flexural strain that intrarift sources in Malawi are accommodating, and which is not directly incorporated into v. We define c_{hwf} as:

$$c_{hwf} = \frac{1}{(T_{if-ext} - hwf_{ext})/T_{if-ext}} \tag{3}$$

where T_{if-ext} is the estimated total cumulative extension across a basin's intrarift sources (Appendix A), and hwf_{ext} is the flexural

345 extension across the basin as modelled following a broken-plate model (Figs. 4 and A3; Tables A2 & A3; Billings and Kattenhorn, 2005; Muirhead et al., 2016; Shillington et al., 2020; Turcotte and Schubert, 1982). The calculated profiles across these basins cannot determine which intrarift sources will accommodate disproportionately more or less flexural strain (Fig. 4), and so each intrarift source in a given basin is assigned the same range of c_{hwf} values. Hanging-wall flexural modelling in the basins south of Lake Malawi indicates negligible flexural extension (<1%) due to the much lower throws (<1 km) on the

350 region's border faults (Fig. A3, Table A2; Bloomfield, 1965; Kolawole et al., 2022; Ojo et al., 2022b), and so c_{hwf} is set to one for these basins.
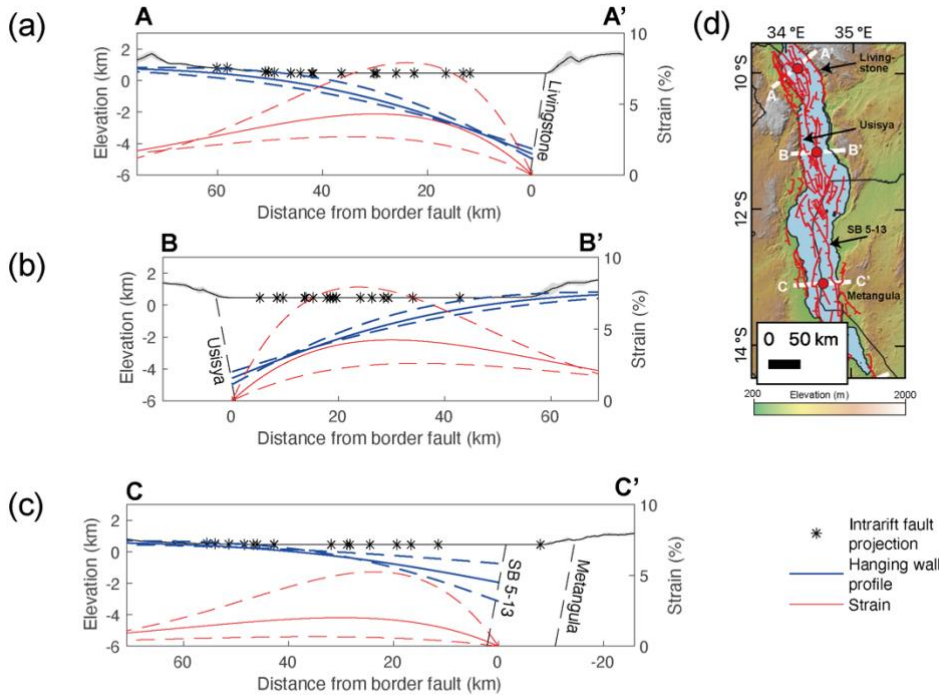
Figure 4: Representative hanging-wall flexural and flexural strain profiles through the (a) North, (b) Central and (c) the South Basins of Lake Malawi. For each profile, a solid line indicates the median value, and dashed lines indicate upper and lower

355 estimates using previous estimates of fault throw (Accardo et al., 2018; Shillington et al., 2020) and the parameters listed in Table A2. Solid black line and gray shading represents mean and one standard deviation topography from (a) SRTM 30 m DEM, and (b&c) TanDEM-X 12 m DEM in 10 km swath (Schwanghart and Scherler, 2014) on profile locations shown in (d).

Profiles have 3x vertical exaggeration. Note, in (c) there is uncertainty about whether flexural strain should be projected from the South Basin 5-13 or Metangula faults, but this does not affect our estimates of the magnitude of flexural strain, or how it may be distributed across different intrarift faults.

3.3 Earthquake magnitudes and recurrence intervals

We apply empirically derived earthquake scaling relationships to estimate the magnitude and average single event displacement of an earthquake along a MSSM source. For consistency with estimates of a source's area, we use the Leonard, (2010) relations to calculate these parameters. Inherent in the Leonard, (2010) magnitude scaling relationships for dip-slip faults are that L_s scales with W following Eq. 1, however, this scaling breaks down for MSSM sources whose down-dip extent is limited by an intersecting source or the thickness of the seismogenic layer (Sect. 3.1.2). We therefore adapt the model that Leonard (2010) applied for width-limited strike-slip ruptures, which indicates that seismic moment (M_0) $\propto L_s^{1.5}$ and $\bar{D} = c_2\sqrt{A_s}$, where A_s is source area and equals $L_s z/sin\delta$, c_2 is an empirically derived constant, and $\bar{D}$ is average single event displacement. The earthquake magnitude of source s in the MSSM therefore equals:

$$M_W(s) = \begin{cases} \frac{\frac{5}{2}logL_s + \frac{3}{2}logc_1 + logc_2\mu - 9.05}{1.5}, & if\ c_1 L_s{}^{2/3} < \frac{z}{\sin\delta} \\ \frac{\frac{3}{2}logA_s + logc_2\mu - 9.05}{1.5}, & for\ truncated\ sources\ or\ if\ c_1 L_s{}^{2/3} > \frac{z}{\sin\delta} \end{cases} \quad (4)$$

and $\bar{D}$ is:

$$\bar{D}(s) = \begin{cases} 10^{\frac{5}{6}logL_s + \frac{1}{2}logc_1 + logc_2\mu}, & if\ c_1 L_s{}^{2/3} < \frac{z}{\sin\delta} \\ c_2\sqrt{A_s}, & for\ truncated\ sources\ or\ if\ c_1 L_s{}^{2/3} > \frac{z}{\sin\delta} \end{cases} \quad (5)$$

where μ is the shear modulus (33 GPa; Leonard, 2010), and z is 35 km, as used in Eq. 1. Estimates of M_W and slip rates are then combined to calculate recurrence intervals (R) through the relationship $R = \bar{D}$ /slip rate (Wallace, 1970).

3.4 Uncertainty in the MSSM

There is considerable uncertainty in the variables used to calculate the slip rate and recurrence interval estimates in the MSSM. For the slip rates derived by Shillington et al., (2020) in the North Basin of Lake Malawi from the offsets on the 75 ka megadrought horizon in seismic reflection data, the primary source of uncertainty is, at these shallow depths, associated with the vertical resolution of the seismic reflection data, which is controlled by the frequency content of the data and the signal - to -noise ratio. The vertical resolution of seismic reflection data is typically estimated to be a quarter of the wavelength ($\lambda/4$) of the seismic data (Widess, 1973), though some authors report detecting faults with much smaller offsets in data with low noise (e.g., $\lambda/30$; Brown, 2011; Faleide et al., 2021). The dominant frequency of the relevant depth range of the seismic reflection data assessed by Shillington et al., (2020) is 40-60 Hz, and so $\lambda\sim$25-37.5 m. For the purposes of this study, we apply

the λ/4 rule, a velocity of 1500 m/s and 50 Hz, which gives an uncertainty of 7.5 m; however, we consider this a very conservative estimate since we can identify much smaller fault offsets in some places. In addition, the reflector's age, which was obtained from Optically Stimulated Luminescence (OSL) dating of a drill-core interval that was tied to the reflector (Scholz et al., 2007), has a ± 5,290 year uncertainty associated with it, and there is a range of plausible fault dips the vertical offset measurement could be projected into (40-65º).

To quantify the uncertainties of these slip rate estimates, we follow the probabilistic framework of Zechar and Frankel, (2009). Specifically, we treat the OSL drill-core date as a normal distribution, and the slip measurement uncertainty (i.e., the combination of the vertical offset and fault dip uncertainties) as a boxcar function. Where multiple offset measurements of the reflector have been made for the same fault, a single offset probability distribution function (*pdf*) is derived from normalizing the sum of the individual offset *pdfs* (Zechar and Frankel, 2009). The resulting slip rate of each fault is then also treated as a normal *pdf*, albeit with a truncation for slip rates <0 (Zechar and Frankel, 2009). For multi-fault sources whose slip rate is measured from the offset reflector, the slip rate and slip rate uncertainty is derived from the area-weighted average slip rate of the participating fault sources.

Uncertainty in the parameters used to estimate slip rates and earthquake recurrence intervals from the systems-based approach is addressed through a logic tree (Fig. 5). A common interpretation of a logic tree is that all possible branch combinations represent a mutually exclusive and collectively exhaustive (MECE) set of events (Bommer and Scherbaum, 2008). However, it is difficult to interpret the results of logic trees using an MECE approach, as strictly speaking it implies that only one (unknown) outcome is correct, and all other branches provide no other information (Bommer and Scherbaum, 2008; Marzocchi et al., 2015). In the MSSM, we therefore sample epistemic uncertainty by incorporating the "relaxed view" of logic trees (Cramer et al., 1996; Gerstenberger et al., 2020; Marzocchi et al., 2015). In this context, uncertainty is defined nonparametrically by the variability of outcomes from the logic tree itself. Specifically, we calculate a slip rate and recurrence interval for each MSSM source in 10,000 Monte Carlo simulations of the logic tree in Fig. 5. We then fit a normal distribution, truncated at values <0, to the slip rate simulation results (Fig. 6a), and since it is calculated through a log function in Eq. 4, a log normal distribution to the recurrence intervals R (Fig. 6b).

When sampling the MSSM logic tree, we treat parameters that have been described by standard deviations (σ) about a mean value as a continuous normal distribution in the simulations (Fig. 5). Parameters assigned based on a range of observed values in Malawi (e.g., fault dip) are discretized into three equally weighted values based on an expert judgement (Fig. 5). We note that there are pitfalls with using expert judgements in logic trees, however, for a tree with many branches, the outcomes are generally insensitive to the weightings, and it is the values at each logic tree step that are of importance (Bommer and Scherbaum, 2008).

420   For simplicity, the slip rate and R reported for each source are the mean values from the distributions fitted to the simulation results, and the upper and lower reported values represent 1σ uncertainty (Fig. 5, Table 1). In this context, the upper and lower values of slip rate and R represent our certainty in these parameters at a 68% confidence level. However, should a MSSM user wish to derive the uncertainty in slip rate and R at different confidence levels, they will be able to do so through the reported values.

425   **3.5 Slip rate comparison**

    There are 11 MSSM fault sources in the north basin of Lake Malawi in which slip rates can be derived from the offset of a 75 ka seismic reflector (Shillington et al., 2020) and from the systems-based approach. Since in both cases, the slip rates are expressed as normal distributions that are truncated for values <0 (Sect. 3.4), we performed the following statistical tests to test how well these independent estimates of fault slip rates compare: (1) a two sample Chi Square (χ^2) test that 600 samples

430   randomly drawn from the slip rate distributions are distinct at a 95% confidence level, and (2) calculation of the overlapping coefficient (*OVL;* Clemons and Bradley, 2000; Inman and Bradley Jr, 1989) between probability distributions $f_1(x)$ and $f_2(x)$:

$$OVL = \int \min[f_1(x), f_2(x)] \cdot dx \tag{6}$$

435
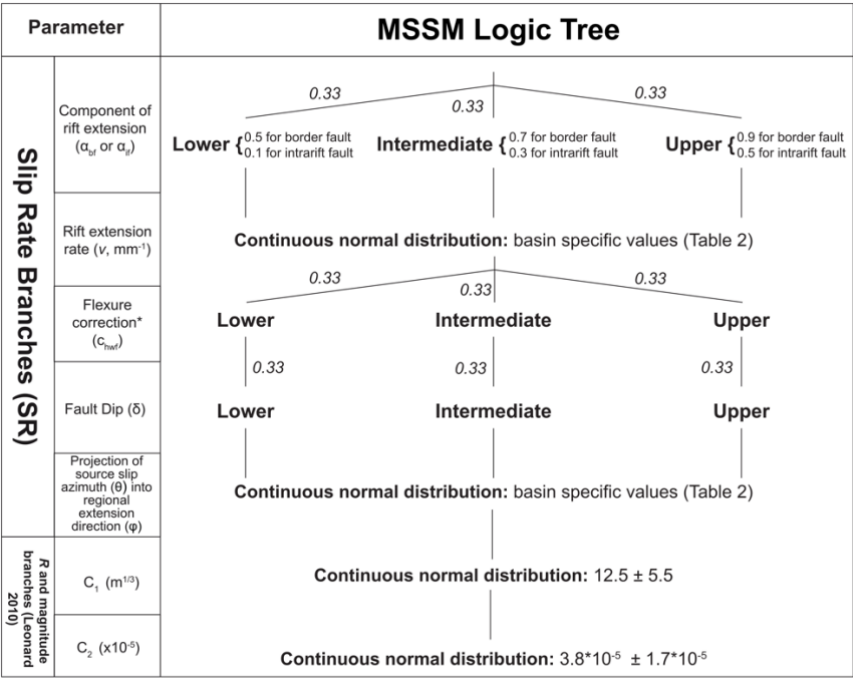
Figure 5: Logic tree branches through which Monte Carlo simulations are performed to describe uncertainty in the MSSM. Continuous parameters are sampled from a normal distribution. If this results in a slip rate <0, the slip rate is truncated

accordingly. Not all possible logic tree branches are represented above. Instead, those from which we can obtain extreme lower, intermediate, and upper slip rate and recurrence interval estimates are shown. *Flexure correction step only performed for intrarift sources in Lake Malawi (Sect. 3.2).

4. Results

4.1 MSSM overview

The Malawi Seismogenic Source Model (MSSM) provides geometric, kinematic, and seismogenic information about 275 possible earthquake sources in Malawi and its surrounding region. These are divided into 108 'fault' sources, 140 'section' sources, and 27 'multi-fault' sources. Mean slip rate estimates are ~0.05-0.3 ± 0.05 mm/yr for intrarift sources and ~0.5-1.5 ±0.3 mm/yr for sources hosted on border fault systems (Fig. 7, Table 3). There is an overall increase in slip rates from south to north Malawi (Fig. 7d-f) due to higher EAR extension rates as distance from the San-Rovuma Euler Pole increases (Fig. 1; Wedmore et al., 2021) and, for intrarift sources, the contribution of hanging-wall flexure to slip (Shillington et al., 2020). There are more multi-fault sources in central and northern Malawi (Fig. 7d-f), although we cannot distinguish whether this reflects how fault tips are mapped in the DEMs and seismic reflection data, or if this reflects that previously distinct faults are beginning to interact and coalesce in this more evolved part of the Malawi Rift.
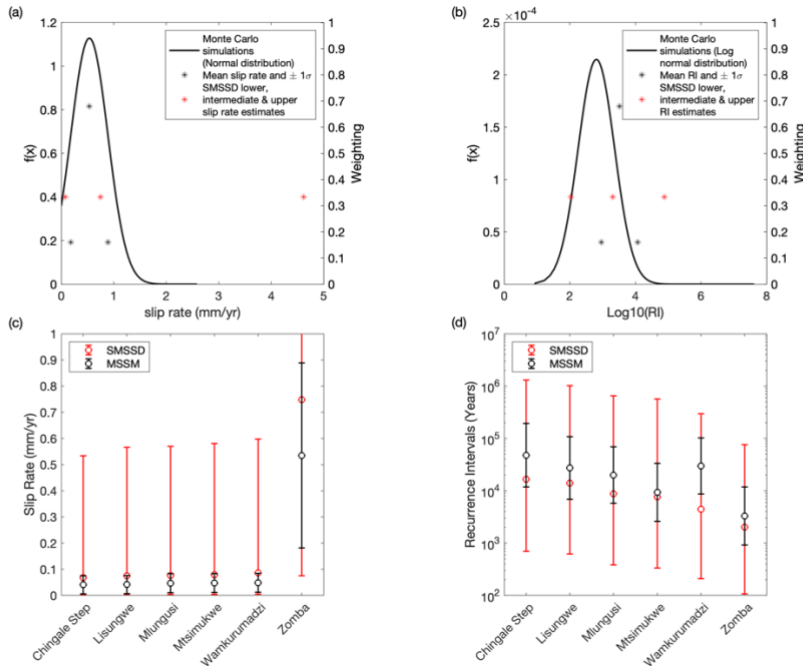
Figure 6: Comparison of uncertainty between the Malawi Seismogenic Source Model (MSSM) and the South Malawi Seismogenic Source Database (SMSSD; Williams et al., 2021a). (a) Slip rate for the Zomba fault modelled from the extreme cases of the logic tree (SMSSD) and from 10,000 Monte Carlo simulations through the logic tree (Fig. 5) and then fit to a

normal distribution truncated at zero (MSSM). For the MSSM, results can also be discretized by the mean value ± 1 standard deviation (σ). For the SMSSD, no weighting was formally assigned to either estimate and so is depicted here as three equal weightings. (b) Equivalent to (a) but for the Zomba Fault recurrence interval (R), which follows a log normal distribution. Comparison of (c) mean slip rate and (d) mean recurrence interval estimates for all faults in the Zomba Graben between the
460   SMSSD and MSSM. Error bars represent extreme values (SMSSD) and 1σ (MSSM).

The mean and range of intermediate earthquake magnitude estimates for section sources in the MSSM is M_W 6.3 and M_W 5.4-7.7, M_W 6.8 and M_W 5.6-7.9 for fault sources, and M_W 7.4 and M_W 6.6-8.1 for multi-fault sources (Fig. 7, Table 3). Twenty-eight sources are identified that are capable of hosting M_W >7.5 earthquakes with the largest magnitude source (M_W 8.1) being
465   the 268 km long South Basin Fault 5-13 multi-fault system (Fig. 2b). If earthquakes in Malawi occur only as 'section' type events, then their recurrence intervals are ~500-30,000 years. Alternatively, if they only occur on fault and multi-fault systems, recurrence intervals are ~1,000-40,000 years (Table 3). In reality, earthquakes in Malawi likely occur as a combination of section, fault, and multi-fault events, and so these recurrence interval estimates are a minimum estimate, and furthermore they assume that the MSSM sources do have any component of aseismic deformation. We discuss this further in Sect. 5.3. The
470   standard deviation (1σ) uncertainties for slip rates are 0.05-0.3 mm/yr and for recurrence intervals, 1σ uncertainty is approximately one order of magnitude (Fig. 6).

Table 3: Range and mean of selected attributes in the MSSM. The reported values are calculated by considering the intermediate estimates from all MSSM sources for the given type. The analysis of recurrence interval intermediates assumes
475   that each source ruptures only in the given type.

MSSM Parameter	Min	Mean	Max
Border fault slip rate (mm/yr)	0.18	0.76	2.0
Intrarift fault slip rate (mm/yr)	0.03	0.13	0.62
Section magnitude	5.4	6.3	7.7
Fault magnitude	5.6	6.8	7.9
Multi-fault magnitude	6.6	7.4	8.1
Section recurrence interval (years)	380	5900	31800
Fault recurrence interval (years)	370	10800	85800

| Multi-fault recurrence interval (years) | 2720 | 12500 | 42600 |

4.2 Slip rate estimate comparisons in Lake Malawi

We find good agreement between the slip rate estimates for 9 out of 11intrarift fault sources in the North Basin of Lake Malawi when independently derived from either the mean slip rate from the 75 ka offset reflector (Shillington et al., 2020) or from the systems-based approach (Fig. 8). Firstly, using a two sample χ^2 test we can only accept the hypothesis that 600 random samples drawn from the two slip rate distributions are independent (at a 95% confidence level) for faults North Basin Fault 14b and 8. Secondly, the overlapping coefficient (OVL) between the two slip rate probability distributions is >0.5 for 9 out of the 11 faults. Thus, although slip rates are higher when estimated from the offset reflector for 10 faults (Fig. 8), this is not statistically significant.
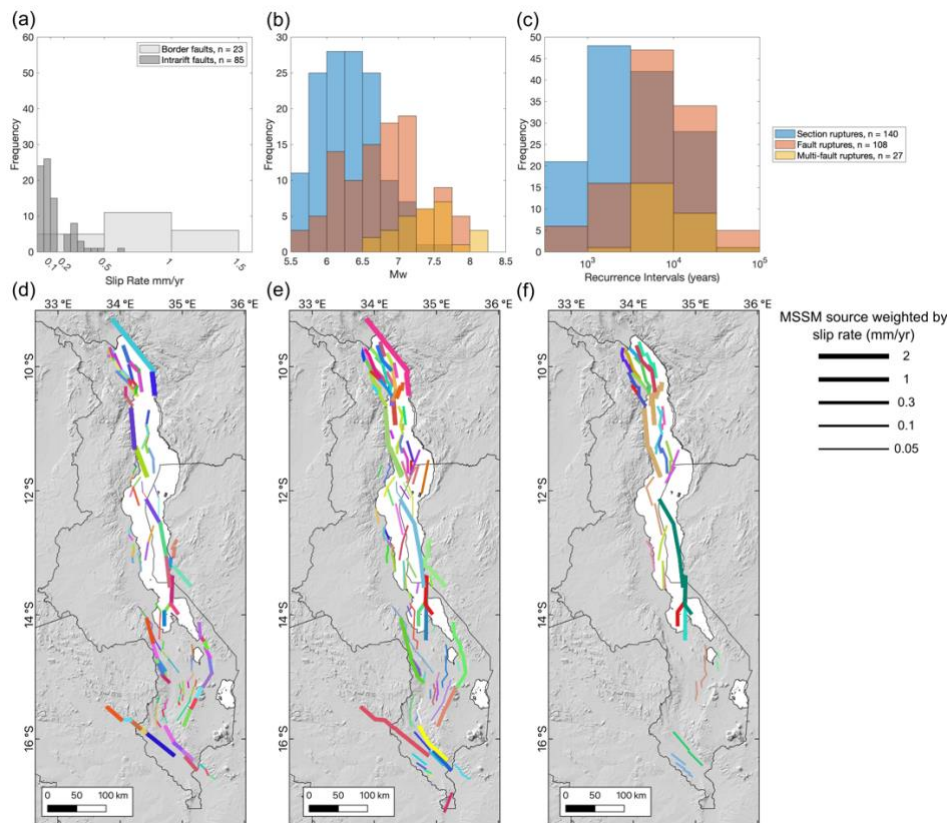
Figure 7: (a-c) Histograms for intermediate estimates of (a) fault slip rates, (b) magnitude estimates, and (c) recurrence intervals in the Malawi Seismogenic Source Database (MSSM). (d-f) Maps of (d) section, (e) fault, and (f) multifault sources in the MSSM, with lines weighted by the source's intermediate slip rate estimate. Each color represents a different source.

The two most difficult slip rate distributions to reconcile are North Basin Fault 14b and Usisya Tip 4 (Fig. 8). In the latter case,

490   this fault represents the northern tip of the Usisya border fault system, and so this result may reflect along-strike reductions in the slip rate of this segmented border fault system (Accardo et al., 2018; Contreras et al., 2000). In the case of North Basin Fault 14b, this has been previously interpreted as a particularly high slip-rate intrarift fault given its 2.5 km total throw (see Fault 1 of Shillington et al., 2020). These comparisons therefore indicate that there is more along- and across-strike variation in the slip rate of intrarift faults in Malawi than suggested by the systems-based approach, where the only parameter that results

495   in slip rate variations within an individual basin is the fault slip azimuth with respect to the regional extension direction (Eq. 2).
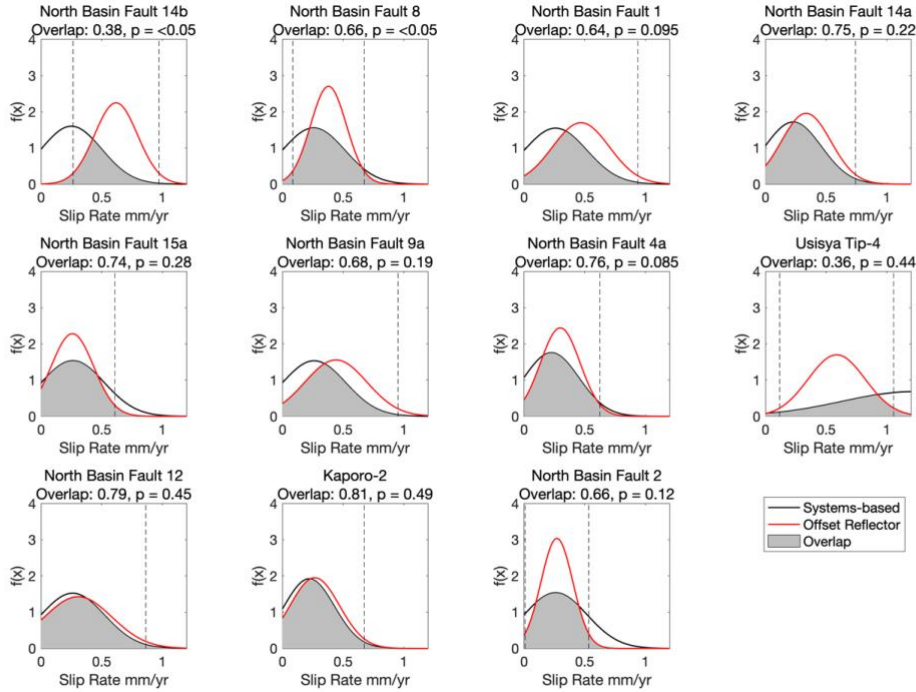
Figure 8: Comparison of the slip rate probability distribution for 11 intrarift faults in the North Basin of Lake Malawi when derived from the 'systems-based' approach and offset seismic reflector (Shillington et al., 2020). Dashed vertical lines indicate

500   two standard deviations about the mean value of the offset-reflector slip rate distributions. For each plot, we report the overlap coefficient (*OVL*) between the two probability distributions (Eq. 6) and the *p*-value from a two-sample χ^2 test on 600 samples randomly drawn from these distributions. The χ^2 test accepts the null hypothesis that there is no difference in these samples when $p > 0.05$.

5. Discussion

5.1 Assessment of fault slip rate estimates in the MSSM

The MSSM uses a new geodetic model for East Africa (Wedmore et al., 2021) compared to that used in the South Malawi Seismogenic Source Database (SMSSD; Saria et al., 2013; Williams et al., 2021b). Overall, the rift extension rates inferred from these models are broadly similar, so using the Wedmore et al., (2021) model does not significantly change the mean slip rate estimate (Fig. 6). However, there is a significant reduction in the regional extension rate uncertainties (from ± 1.5 mm/yr to ± 0.3 mm/yr, Table 2). This demonstrates the importance of collecting new geodetic data in East Africa to reduce epistemic uncertainty in seismic hazard assessment.

By using the variability of logic tree outcomes to describe slip rates and recurrence intervals in the MSSM, we also provide a more thorough description of the epistemic uncertainty in these parameters than the SMSSD, which considered the extreme and intermediate logic tree branches only (Fig. 6c&d; Williams et al., 2021a). This approach could be used to model uncertainty in other regions where alternative hypotheses for slip rates and recurrence intervals have been explored using logic trees (Beauval et al., 2018; Vallage and Bollinger, 2020). Nevertheless, no MSSM slip rate estimates are 'well-constrained' under the test that a well-constrained slip rate is one where the median estimate is greater than the width of its 95% confidence interval (Bird and Liu, 2007; Zechar and Frankel, 2009).

When estimated from the offset of a 75 ka seismic reflector (Shillington et al., 2020) and the systems based approach (Eq. 2; Williams et al., 2021a), the slip rate probability distribution of intrarift faults in the North Basin of Lake Malawi are not statistically distinct for 9 out of 11 faults (Fig. 8). The fault slip rates we obtain are also comparable to estimates obtained from apatite fission track modelling of footwall uplift in southern Malawi (Ojo et al., 2022a). This suggests that the systems-based approach is an appropriate method to estimate faults slip rates in Malawi where no other constraints are currently available. Nevertheless, the large uncertainties in the slip rate probability distributions highlight the need to collect new geologic and geodetic data in Malawi to refine these estimates.

5.2 Earthquake magnitude estimates in the MSSM

There are 28 sources in the MSSM that, given their geometry and the Leonard, (2010) scaling relationships (Eq. 4), can host M_W >7.5 earthquakes. If such an event was to occur, it would be amongst the largest recorded continental normal fault earthquakes (Middleton et al., 2016; Valentini et al., 2020; Xu et al., 2018). Indeed, it has been questioned whether M_W >7.5 continental normal fault earthquakes are physically possible due to the constraints imposed by smaller differential stresses and rupture widths in continental crust where the seismogenic layer is typically 10-20 km thick (Neely and Stein, 2021; Xu et al., 2018). However, we suggest that these factors do not limit earthquake magnitudes in Malawi given its cold, anhydrous, frictionally strong, and thick seismogenic layer (35 km; Ebinger et al., 2019; Fagereng, 2013; Hellebrekers et al., 2019; Jackson

and Blenkinsop, 1993, 1997; Stevens et al., 2021). Furthermore, geomorphic analysis of the Billila-Mtakataka Fault scarp indicates high single event displacements (~5-10 m), which is consistent with it hosting M_W 7.4-8.0 earthquakes (Hodge et al., 2020). We also note our magnitude estimates are contingent on the hypothesis that source width will saturate at L_s >140 km

540 so that $M_0 \propto L_s^{1.5}$ (Leonard, 2010; Sect. 3.1.2). However, we cannot exclude the possibility that very long ruptures propagate below 35 km. If true, then the MSSM underestimates magnitudes for sources with lengths >140 km

5.3 Future directions for the MSSM

As 'section,' 'fault,' and 'multifault' sources are mutually exclusive, in future, weightings could be assigned to each source to indicate their relative likelihood. Future updates to the MSSM may also consider that: 1) the MAFD is not a complete database
545 of active faults in Malawi; particularly faults <10 km long, or faults that do not show evidence for EAR displacement but that are still active (Williams et al., 2022b), 2) there is uncertainty in how faults should be extrapolated down-dip and/or intersect at depth in Malawi, and 3) the MSSM does not contain information about potential earthquakes that rupture multiple sections but not the whole length of a segmented fault. Indeed, earthquakes are not necessarily predisposed to conform to fault segment boundaries identified from empirically derived geometrical criteria (Kagan et al., 2012). Cumulatively, these challenges could
550 be explored by weighting different MSSM source types so that the seismicity they produce fits a target regional magnitude frequency distribution (Chartier et al., 2017), or by geometrically subdividing the sources and randomly 'floating' ruptures of any size to fit a magnitude-frequency distribution (Field et al., 2014; Visini et al., 2020).

It is implicit in the MSSM approach that the slip rate assigned to each source is released seismically (i.e., the seismic coupling
555 coefficient (c) in Malawi is equal to 1). This is consistent with observations of earthquakes nucleating across its 30-40 km thick seismogenic layer (Ebinger et al., 2019; Stevens et al., 2021) and the velocity weakening behaviour of representative basement samples from Malawi in deformation experiments at lower crustal pressures and temperatures (Hellebrekers et al., 2019). However, some shallow (depths <6 km) aseismic deformation was observed in northern Malawi following a M_W 5.2 earthquake in 2014 (Zheng et al., 2020). Obtaining a more representative estimate of c in Malawi could be achieved through a
560 comparison of its geodetic and seismic moment rate. However, the short duration of the instrumental catalog in Malawi would make this comparison challenging (Hodge et al., 2015). Reconciling seismic and geodetic moment rates in Malawi, weighting different source types, and allowing sources in the MSSM to exhibit a more diverse set of earthquake ruptures, are being considered in an ongoing new fault-based PSHA for Malawi (Williams et al., 2022a).

6. Conclusions

565 The Malawi Seismogenic Source Model (MSSM) is a freely available database that documents the geometry, slip rate, and earthquake magnitude and recurrence intervals of 275 possible earthquake sources in Malawi and neighboring Tanzania and Mozambique. It is distinct, but complementary to the Malawi Active Fault Database (Williams et al., 2022b). The MSSM also represents an update of the South Malawi Seismogenic Source Database (Williams et al., 2021a) due to the application of a

new geodetic model (Wedmore et al., 2021), new active fault mapping (Kolawole et al., 2021a), and a more robust description
570 of uncertainty.

The >100 km length-scale of faults and multi-fault sources in the MSSM imply that Malawi may experience earthquakes M_W >7.5. Such magnitudes, although rare for continental normal faults, are consistent with the crust's rheology in Malawi. Regional extensional rates of 0.5-1.5 mm/yr imply the occurrence of such large magnitude events will be low (10^3-10^4 years);
575 however, the MSSM also documents the possibility of M_W 5.5-6.5 earthquakes with recurrence intervals of ~10^3 years, and such events can also cause significant loss in Malawi (Goda et al., 2016; Gupta and Malomo, 1995). A workflow to use the MSSM in probabilistic seismic hazard analysis is currently in development (Williams et al., 2022a).

Slip rates in the MSSM are estimated from either a systems-based approach that derives these rates from partitioning regional
580 geodetic extension rates across faults, or, in Lake Malawi, direct measurements from the offset of a 75 ka seismic reflector (Shillington et al., 2020). Where it is possible to compare these estimates, we find the slip rate probability distributions are not significantly distinct (at a 95% confidence level) for 9 out of the 11 assessed faults. This suggests that the slip rates (~0.05-3 mm/yr) estimated elsewhere in Malawi from partitioning extension rates are meaningful. Hence, combining geodetic data with geological theory on regional strain distribution, active fault maps, and earthquake scaling relationships can provide important
585 insights into the seismic hazard of other regions lacking historical or paleoseismic records.

Appendix

Below we provide an additional table and figure that provide extra detail to this study. A description of the hanging-wall flexural analysis is then provided in Appendix A.

590 **Table A1**: List of faults that are included in the Malawi Active Fault Database (MAFD; Williams et al., 2022b), but not the Malawi Seismogenic Source Database (MSSM). The reason for their removal from the MSSM is also listed.

Fault	Reason for not including in the MSSM
Nchalo	NW dip implies intersection with the Thyolo Fault with <6 km across strike distance
Mudi	Closely spaced (2 km) across strike from the Thyolo Fault, possible splay
Jimbe	Closely spaced (2 km) across strike from the Lisungwe Fault, possible splay
Chileka	Closely spaced (5 km) across strike from the Zomba Fault, possible splay

Nguluwe	Closely spaced (5 km) across strike from the Zomba Fault, possible splay
Lirangwe River	<5 km long
Linjidzi	<5 km long
Ngondo-1	<5 km long
Ngondo-2	<5 km long
Namiyala-1	Part of closely (<2 km) fault system at a bend in the Makanjira Fault. Likely a splay of this larger fault system
Namiyala-2	Part of closely (<2 km) fault system at a bend in the Makanjira Fault. Likely a splay of this larger fault system
Namiyala-3	Part of closely (<2 km) fault system at a bend in the Makanjira Fault. Likely a splay of this larger fault system
Chilongwelo	E dip implies intersection with the South Basin 5-13 Fault system with <6 km across strike distance
Leopard Bay-2	<5 km long
South Basin Fault 4	E dip implies intersection with the South Basin 3 Fault with <6 km across strike distance
Central Basin Fault 4	W dip implies intersection with Central Basin 6 Fault with <6 km across strike distance
Central Basin Fault 9	Interpreted as linking structure between Central Basin Faults 9 and 22
Central Basin Fault 10	W dip implies intersection with Central Basin 11 Fault with <6 km across strike distance
Central Basin Fault 22	W dip implies intersection with Central Basin 20 Fault with <6 km across strike distance
Hara Plain	<5 km long

| South Karonga East | W dip implies intersection with South Karonga West Fault with <6 km across strike distance |
| Lupaso | E dip implies intersection with Katesula Fault with <6 km across strike distance |
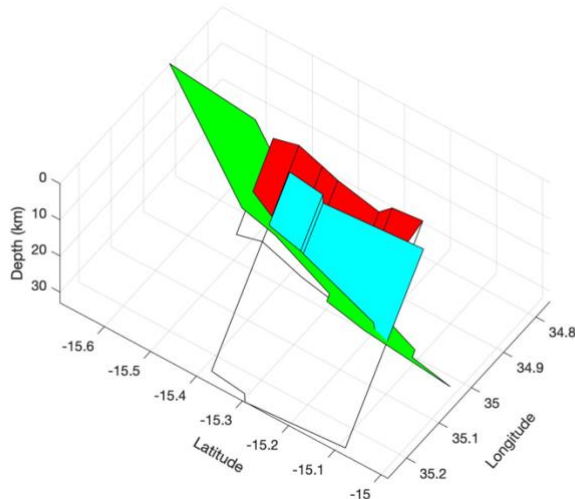
Figure A1: Examples of faults in the MSSM that are projected to intersect and where the across strike distance at the surface is sufficient (>6 km) that they are interpreted to represent distinct sources. In this case the longer Chingale Step fault (green) is interpreted to have cut off the shorter Mlungusi (red) and Liwawadzi (cyan) faults, so that their geometry does not extend below the intersection, as indicated by transparent polygons. The revised cut off area of these faults is then used in the earthquake magnitude and single event displacement scaling relationships (Eqs. 4 and 5 in the main text).

Hanging-wall flexure in Malawi

The considerable amounts of throw (>1000 m) along a rift bounding fault can induce a significant amount of flexure within the lithosphere either side of the fault (Muirhead et al., 2016; Olive et al., 2014; Petit and Ebinger, 2000; Shillington et al., 2020). In the case of the hanging-wall, this is a downward flexure that can result in intrabasinal faults accommodating additional slip to that imparted by regional extension alone (Muirhead et al., 2016). This additional flexural strain must therefore be accounted for when considering the slip rate of faults in Malawi (Sect. 3.2, main text).
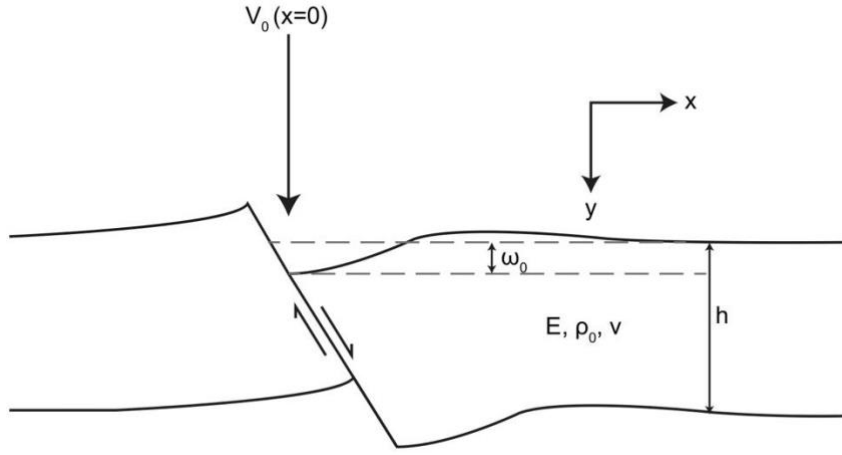
Figure A2: Set-up for hanging wall deflection equations. A vertical load (V_0) is applied to the point where the hanging-wall intersects the surface (i.e., where $x=0$) and where there is a maximum deflection (ω_0). The elastic thickness, Young's Modulus, density, and Poisson's ratio of the crust are represented by h, E, ρ_0, and v respectively.

610

The influence of flexural strain on basement profiles across the Lake Malawi basins has been previously assessed (Shillington et al., 2020) using the Broken Plate model (Billings and Kattenhorn, 2005; Muirhead et al., 2016; Turcotte and Schubert, 1982) and we report the values used to generate representative profiles across these basins in Fig. 4 in the main text. In addition, we apply the Broken Plate model to provide the first estimates of hanging-wall flexural strain in southern Malawi. Unlike in Lake

615 Malawi, there is little subsurface data to validate the resulting profiles in this region, and there is additional complexity due to intrarift topography (e.g. Shire Horst, Kirk Range) and possible rift-widening events such as when the Lower Shire Basin was reactivated during East African Rifting (Castaing, 1991; Kolawole et al., 2022). Therefore, the purpose of these profiles is not to precisely model the across-rift basement geometry, but to estimate the range of hanging-wall flexural extension that may have occurred in southern Malawi given the uncertainty of each parameter we must test. This analysis is conducted only for

620 the Makanjira, Zomba, and Lower Shire basins, as no intrarift faults have been identified in the Lengwe and Nsanje basins (Williams et al., 2022b).

The Broken Plate model calculates flexure by considering a vertical line-load at the point of maximum deflection (i.e., at the upper contact of the border fault hanging wall, Fig. A2). The deflection (ω) across a border fault hanging wall can then be

625 estimated as:

$$\omega = \omega_0 e^{\frac{-x}{\alpha}} \cos\left(\frac{x}{\alpha}\right) \tag{A1}$$

where ω_0 is the maximum deflection, x is the position along a hanging wall profile from the deflecting fault (Fig. A2), and α is:

$$630 \quad \alpha = \left[\frac{Eh^3}{(3\rho_0 g(1-v^2))}\right]^{\frac{1}{4}} \tag{A2}$$

where E is Young's Modulus, v is Poisson's ratio (0.25), g is acceleration due to gravity (9.8 m/s^2), h is the thickness of elastic crust, which is assumed here to be the equivalent to the thickness of Malawi's seismogenic layer. and ρ_0 is crustal density, for which the average crustal density (2816 kg/m3) from a Malawi three layer model is used (Fagereng, 2013; Nyblade and Langston, 1995). Shillington et al., (2020) applied a value of E (3 ± 1.5 GPa) such that the hanging wall deflection is restricted

635 to a distance comparable to the actual width of Lake Malawi's basins, and we apply this value to south Malawi.

Table A2: Inputs and results of hanging-wall flexure analysis across Malawi. ω_0; maximum hanging-wall deflection calculated from Eq. A3

Basin	Sediment thickness (m)	Escarpment height (m)	Border fault throw (m)	Maximum Deflection, ω_0 (m)	Elastic plate thickness (km)	Young's Modulus (GPa)	Mean extension (%)	Basin Width (km)	Total horizontal extension (km)
North[a]			6400±400[b]	5120±320	38±3	3±1.5	$3.3^{-1.3}_{+2.4}$	60	$2.0^{-0.8}_{+1.4}$
Central[a]			6300±500[b]	5040±400	38±3	3±1.5	$3.3^{-1.3}_{+2.7}$	50	$1.6^{-0.6}_{+1.4}$
South[a]			3000±1500	2400±1200	38±3	3±1.5	$1.5^{-1.0}_{+2.0}$	50	$1.0^{-0.7}_{+1.4}$
Makanjira East (Makanjira)	70±40[c]	400±100[e]	470±140	370±110	32.5±2.5	3±1.5	$0.7^{-0.4}_{+0.6}$	90	$0.6^{-0.3}_{+0.6}$
Makanjira West (Chirobwe -Ncheu & BMF)	300±200[c]	850±150[e]	1150±350	920±280	32.5±2.5	3±1.5			

Zomba	50±15[d]	300±100[e]	350±115	280±90	32.5±2.5	3±1.5	0.2±0.1	60	$0.1_{+0.1}^{-0.05}$
Lower Shire	900±300[f]	750±250[g]	1650±550	1320±440	32.5±2.5	3±1.5	$0.9_{+1.1}^{-0.5}$	40	$0.4_{+0.5}^{-0.2}$

[a]Profiles based on previous hanging-wall flexural analysis in Shillington et al., (2020).

[b]Border fault throw estimates from Accardo et al., (2018).

[c]Thickness of sediments in the hanging-wall of the Chirobwe-Ncheu and Bilila-Mtakataka faults (BMF) based on electrical resistivity surveys, depth to magnetic basement in aeromagnetic data and basement penetrating boreholes (Fig. A3; Bloomfield and Garson, 1965; Ojo et al., 2022b; Walshaw, 1965).

[d]Thickness of sediments from borehole data within the Shire Plain (Fig. A3; Bloomfield and Garson, 1965).

[e]See Laõ-Dávila et al., (2015). For the Zomba fault, topography associated with Chilwa Alkaline Province intrusion at the northern end of the fault is removed. Escarpment height from Chirbowe-Ncheu Fault also includes escarpment height of the Bilila-Mtakataka Fault.

[f]Based on range of depth to magnetic basement values in the Thyolo Fault hanging-wall (Kolawole et al., 2022).

[g]See Wedmore et al., (2020b).

In Eq. A1, ω_0 can be derived through the observation from real and modelled normal faults that the ratio (r) of upthrow to downthrow along a normal fault is typically 0.2 (Muirhead et al., 2016). Therefore:

$$\omega_0 = BF_{throw}(1 - r) \tag{A3}$$

where BF_{throw} is border fault throw and is equivalent to the sum of the footwall escarpment height and hanging wall sediment thickness. In the onshore basins in southern Malawi, hanging-wall sediment thickness is constrained by a combination of basement-penetrating boreholes aeromagnetic data, and electrical resistivity surveys (Table A2; Figure A3; Bloomfield, 1965; Bloomfield and Garson, 1965; Habgood et al., 1973; Kolawole et al., 2022; Ojo et al., 2022b; Walshaw, 1965).

Given a profile of hanging wall deflection, it is possible to derive the resulting flexural extensional strain (ε) within a half-graben (Billings and Kattenhorn, 2005; Muirhead et al., 2016)

$$\varepsilon = -y\left(\frac{d^2\omega}{dx^2}\right) \tag{A4}$$

where y is the vertical distance from the centre of the plate (downward is positive, Fig. A2). Following Muirhead et al., (2016) and Shillington et al., (2020), we report the flexural strain in terms of the average strain across each basin, and multiply this

by basin width to get extension (Table A2). For the Makanjira graben, we calculate the mean strain from the contribution of

665 each side of the graben over its 90 km width (i.e., for the Chirobwe Ncheu and Makanjira faults, Fig A3, Table S2).

Results of this analysis are shown in Figs. 4 (Lake Malawi basins), A3 (south Malawi basins), and Table A2. These demonstrate that regardless of the simplifications, uncertainties and assumptions in this analysis, hanging-wall flexure in southern Malawi is negligible (strains <1%) compared to the Lake Malawi basins. Furthermore, unlike the Lake Malawi basins, the flexural

670 profiles in southern Malawi do not match the observed topography (Fig. A3), which further indicates minimal flexural extension in these basins. This result reflects the significant differences in total rift extension between the South Basin and Makanjira Graben and resulting reduction in border fault throw between these basins (Table A2). We therefore do not consider hanging-wall flexure further when considering the slip rate of intrarift sources in southern Malawi (Sect. 3.2, main text).
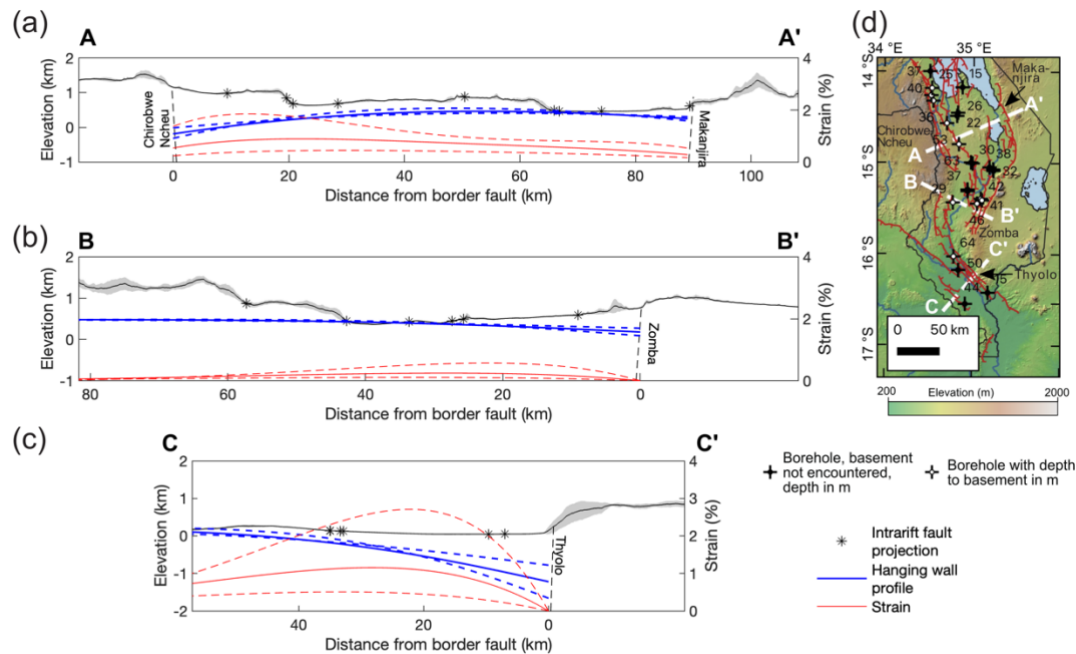
675 **Figure A3**: Modelled hanging-wall flexural profiles and horizontal extensional strain in southern Malawi. Profiles have 6x vertical exaggeration. Calculated following broken plate model (Fig. A2; Billings and Kattenhorn, 2005; Muirhead et al., 2016; Turcotte and Schubert, 1982) and parameters listed in Table A2. Solid hanging-wall profile and strain line indicates median estimates, dashed line indicates maximum and minimum estimates. Solid black line and gray shading represents mean and one standard deviation topography from TanDEM-X 12 m DEM in 10 km swath centred on lines shown in (d) (Schwanghart and

680 Scherler, 2014). Labelled faults indicate border faults. In (d)), the location and depth to basement in boreholes in south Malawi are also shown (Bloomfield and Garson, 1965; Habgood, 1963; Habgood et al., 1973; Walshaw, 1965; Walter, 1972). Map underlain by 30 m resolution Shuttle Radar Topographic Mission digital elevation model.

The higher hanging-wall flexural strain in the Lake Malawi basins (~1-3%, Table A2) suggest that the hanging-wall flexural extension correction factor (c_{hwf}) should be applied when estimate slip rates of their intrarift sources in the MSSM (Eqs. 2 and 3 in the main text). This factor is derived by combining a basin's hanging-wall flexural extension (Tables A2 and A3) with the total cumulative extension accommodated by its intrarift faults ($T_{if\text{-}ext}$, eq. 3 in the main text). This parameter is poorly constrained, and so we make the following assumptions when deriving $T_{if\text{-}ext}$:

- For intrarift faults in the North Basin, the total observed cumulative extension is 2 ± 0.4 km, however, it is estimated that 30% of the extension in the basin may be accommodated by faults below the resolution of the seismic survey (Shillington et al., 2020). Therefore, the total extension of intrarift faults under Lake Malawi's North Basin is estimated to be 2.6 ± 0.5 km. There are three onshore intrarift fault/multifault sources in the North Basin (Fig. 2a). If it assumed that they have accommodated a similar amount of extension as the four offshore fault/mulitfault sources, then their total extension is 1.5 ± 0.3 km, and hence $T_{if\text{-}ext}$, for the North Basin is 4.1 ± 0.8 km.

- No estimates exist for the total observed cumulative extension of intrarift faults under Lake Malawi in the Central and South Basins. However, we note that the Central Basin's age, and flexural and total extension (7.0 vs 6.3 km; Scholz et al., 2020) are very similar to the North Basin. We therefore assume that the Central Basin's sub-lacustrine intrarift faults have accommodated the same amount of extension as the North Basin's, and then apply the same workflow to calculate $T_{if\text{-}ext}$, although in this case there are two and ten onshore and offshore intrarift fault/multifault sources respectively (Table A3).

- Flexural and total extension estimates in the South Basin are approximately 50% of the values for the Central and North Basins (~6-7 km vs 3.7 km; Scholz et al., 2020). We adjust the total extension of sub-lacustrine intrarift faults in the South Basin accordingly and note there are seven and eight onshore and offshore intrarift fault/multifault sources respectively (Table A3).

- Within the uncertainty of the hanging-wall flexural profiles across the Lake Malawi basins, it is possible that all the intrarift fault displacement can be accounted for by hanging-wall flexure alone (i.e., $c_{hwf} \to \infty$). However, we do not consider this a realistic scenario since other factors (e.g., structural inheritance) will cause intrarift faults to accommodate regional rift extension prior to significant flexural extension (Kolawole et al., 2021b; Wedmore et al., 2020a) and so c_{hwf} is truncated at values >5.

Table A3: Values used to derive the hanging-wall correction factor (c_{hwf}, Eq. 3) in slip rate calculations (Eq. 2) for intrarift sources in the North, South, and Central basins. Workflow is discussed in Appendix A text.

Basin	Cumulative lake fault extension (km)	Subseismic fault correction (m)	Onshore fault extension	Total intrarift	Hanging-wall flexure	Hanging-wall flexure

				fault extension	extension (km)	correction factor (c_{hwf})
North Basin	2 ± 0.4	2.6 ± 0.5	1.5 ± 0.3	4.1 ± 0.8	$2.0_{+1.4}^{-0.8}$	$2.0_{+3.0}^{-0.7}$
Central Basin	2 ± 0.4	2.6 ± 0.5	0.4 ± 0.1	3.0 ± 0.6	$1.6_{+1.4}^{-0.6}$	$2.2_{+2.8}^{-0.9}$
South Basin	1 ± 0.4	1.3 ± 0.5	0.9 ± 0.4	2.2 ± 0.9	$1.0_{+1.4}^{-0.7}$	$1.9_{+3.1}^{-0.8}$

Data availability

715 The most recent version (v1.1.) of the Malawi Seismogenic Source Model (MSSM) is available at https://doi.org/10.5281/zenodo.5599616. The MSSM is also available through Github where any changes will be archived and users can suggest changes (https://github.com/LukeWedmore/malawi_seismogenic_source_model). Significant changes will result in a new release at the above DOI. The Malawi Active Fault Database can be accessed at https://github.com/LukeWedmore/malawi_active_fault_database and https://doi.org/10.5281/zenodo.5507189.

720

Code availability

The codes, written in MATLAB, that are used to perform the hanging-wall flexure analysis and calculate the geometry, slip rate, and recurrence interval of the MSSM sources as described in Sect. 3 are available at: https://github.com/jack-williams1/Malawi_PSHA. These codes are part of a larger library that are using the MSSM to perform a probabilistic seismic

725 hazard analysis for Malawi, and is described in Williams et al., (2022a).

Author Contributions

Conceptualization: JW, LNJW, AF, and JB. Data curation: JW and LNJW. Methodology: all authors. Formal analysis: JW, LNJW, DS, CS, and LJMW. Funding acquisition: JB, AF, and MW. Writing – original draft preparation: JW. Writing - review and editing: all authors.

Competing interests

The authors declare that they have no conflict of interest.

Acknowledgements

This work is supported by the EPSRC-Global Challenges Research Fund PREPARE (EP/P028233/1) and SAFER-PREPARED (part of the 'Innovative data services for aquaculture, seismic resilience and drought adaptation in East Africa' grant; EP/T015462/1) projects. We thank Luigi Ferranti and an anonymous reviewer for their insightful comments on this study.

References

Accardo, N. J., Shillington, D. J., Gaherty, J. B., Scholz, C. A., Nyblade, A. A., Chindandali, P. R. N., Kamihanda, G., McCartney, T., Wood, D. and Wambura Ferdinand, R.: Constraints on Rift Basin Structure and Border Fault Growth in the Northern Malawi Rift From 3-D Seismic Refraction Imaging, J. Geophys. Res. Solid Earth, 123(11), 3-10,10,25, doi:10.1029/2018JB016504, 2018.

Accardo, N. J., Gaherty, J. B., Shillington, D. J., Hopper, E., Nyblade, A. A., Ebinger, C. J., Scholz, C. A., Chindandali, P. R. N., Wambura-Ferdinand, R., Mbogoni, G., Russell, J. B., Holtzman, B. K., Havlin, C. and Class, C.: Thermochemical Modification of the Upper Mantle Beneath the Northern Malawi Rift Constrained From Shear Velocity Imaging, Geochemistry, Geophys. Geosystems, 21(6), 1–19, doi:10.1029/2019GC008843, 2020.

Acocella, V., Faccenna, C., Funiciello, R. and Rossetti, F.: Sand-box modelling of basement-controlled transfer zones in extensional domains, Terra Nov., 11(4), 149–156, doi:10.1046/j.1365-3121.1999.00238.x, 1999.

Agostini, A., Bonini, M., Corti, G., Sani, F. and Mazzarini, F.: Fault architecture in the Main Ethiopian Rift and comparison with experimental models: Implications for rift evolution and Nubia-Somalia kinematics, Earth Planet. Sci. Lett., 301(3–4), 479–492, doi:10.1016/j.epsl.2010.11.024, 2011.

Ambraseys, N. N.: The Rukuwa Earthquake of 13 December 1910 In East-Africa, Terra Nov., 3(2), 202–211, doi:10.1111/j.1365-3121.1991.tb00873.x, 1991.

Ambraseys, N. N. and Adams, R. D.: Reappraisal of major African earthquakes, south of 20°N, 1900-1930, Nat. Hazards, 4, 389–419, doi:10.1016/0040-1951(92)90036-6, 1991.

Ayele, A. and Kulhanek, O.: Reassessment of source parameters for three major earthquakes in the East African rift system from historical seismograms and bulletins, Ann. di Geofis., 43(1), 81–94, doi:10.4401/ag-3627, 2000.

Baize, S., Nurminen, F., Sarmiento, A., Dawson, T., Takao, M., Scotti, O., Azuma, T., Boncio, P., Champenois, J., Cinti, F. R., Civico, R., Costa, C., Guerrieri, L., Marti, E., McCalpin, J., Okumura, K. and Villamor, P.: A worldwide and unified database of surface ruptures (SURE) for fault displacement hazard analyses, Seismol. Res. Lett., 91(1), 499–520,

760   doi:10.1785/0220190144, 2019.

Basili, R., Valensise, G., Vannoli, P., Burrato, P., Fracassi, U., Mariano, S., Tiberti, M. M. and Boschi, E.: The Database of Individual Seismogenic Sources (DISS), version 3: Summarizing 20 years of research on Italy's earthquake geology, Tectonophysics, 453(1–4), 20–43, doi:10.1016/j.tecto.2007.04.014, 2008.

Beauval, C., Marinière, J., Yepes, H., Audin, L., Nocquet, J. M., Alvarado, A., Baize, S., Aguilar, J., Singaucho, J. C. and
765   Jomard, H.: A new seismic hazard model for ecuador, Bull. Seismol. Soc. Am., 108(3), 1443–1464, doi:10.1785/0120170259, 2018.

Bendick, R., Bilham, R., Freymueller, J., Larson, K. and Yin, G.: Geodetic evidence for a low slip rate in the Altyn Tagh fault system, Nature, 404(6773), 69–72, doi:10.1038/35003555, 2000.

Bhat, H. S., Olives, M., Dmowska, R. and Rice, J. R.: Role of fault branches in earthquake rupture dynamics, J. Geophys. Res.
770   Solid Earth, 112(11), 1–16, doi:10.1029/2007JB005027, 2007.

Biasi, G. P. and Wesnousky, S. G.: Steps and gaps in ground ruptures: Empirical bounds on rupture propagation, Bull. Seismol. Soc. Am., 106(3), 1110–1124, doi:10.1785/0120150175, 2016.

Biasi, G. P. and Wesnousky, S. G.: Bends and Ends of Surface Ruptures, Bull. Seismol. Soc. Am., 107(6), 2543–2560 [online] Available from: http://dx.doi.org/10.1785/0120160292, 2017.

775   Biggs, J., Nissen, E., Craig, T., Jackson, J. and Robinson, D. P.: Breaking up the hanging wall of a rift-border fault: The 2009 Karonga earthquakes, Malawi, Geophys. Res. Lett., 37(11), doi:10.1029/2010GL043179, 2010.

Billings, S. E. and Kattenhorn, S. A.: The great thickness debate: Ice shell thickness models for Europa and comparisons with estimates based on flexure at ridges, Icarus, 177(2), 397–412, doi:10.1016/j.icarus.2005.03.013, 2005.

Bird, P. and Liu, Z.: Seismic hazard inferred from tectonics: California, Seismol. Res. Lett., 78(1), 37–48,
780   doi:10.1785/gssrl.78.1.37, 2007.

Bloomfield, K.: The Geology of the Zomba Area, Bull. Geol. Surv. Malawi, 16, 1965.

Bloomfield, K. and Garson, M. S.: The Geology of the Kirk Range-Lisungwe Valley Area, Bull. Geol. Surv. Malawi, 17, 1965.

Bommer, J. J. and Scherbaum, F.: The use and misuse of logic trees in probabilistic seismic hazard analysis, Earthq. Spectra, 24(4), 997–1009, doi:10.1193/1.2977755, 2008.

785   Bormann, J. M., Hammond, W. C., Kreemer, C. and Blewitt, G.: Accommodation of missing shear strain in the Central Walker Lane, western North America: Constraints from dense GPS measurements, Earth Planet. Sci. Lett., 440, 169–177, doi:10.1016/j.epsl.2016.01.015, 2016.

Brown, A. R.: Structural Interpretation, in Interpretation of Three-Dimensional Seismic Data, Seventh edition, pp. 61–102, Society of Exploration Geophysicists and American Association of Petroleum Geologists., 2011.

790   Castaing, C.: Post-Pan-African tectonic evolution of South Malawi in relation to the Karroo and recent East African rift systems, Tectonophysics, 191(1–2), 55–73, doi:10.1016/0040-1951(91)90232-H, 1991.

Chartier, T., Scotti, O., Lyon-Caen, H. and Boiselet, A.: Methodology for earthquake rupture rate estimates of fault networks: Example for the western Corinth rift, Greece, Nat. Hazards Earth Syst. Sci., 17, 1857–1869, doi:10.5194/nhess-17-1857-2017,

2017.

795 Chisenga, C., Dulanya, Z. and Jianguo, Y.: The structural re-interpretation of the Lower Shire Basin in the Southern Malawi rift using gravity data, J. African Earth Sci., 149(September), 280–290, doi:10.1016/j.jafrearsci.2018.08.013, 2019.

Christophersen, A., Litchfield, N., Berryman, K., Thomas, R., Basili, R., Wallace, L., Ries, W., Hayes, G. P., Haller, K. M., Yoshioka, T., Koehler, R. D., Clark, D., Wolfson-Schwehr, M., Boettcher, M. S., Villamor, P., Horspool, N., Ornthammarath, T., Zuñiga, R., Langridge, R. M., Stirling, M. W., Goded, T., Costa, C. and Yeats, R.: Development of the Global Earthquake

800 Model's neotectonic fault database, Nat. Hazards, 79(1), 111–135, doi:10.1007/s11069-015-1831-6, 2015.

Clemons, T. E. and Bradley, E. L.: Nonparametric measure of the overlapping coefficient, Comput. Stat. Data Anal., 34(1), 51–61, doi:10.1016/S0167-9473(99)00074-2, 2000.

Contreras, J., Anders, M. H. and Scholz, C. H.: Growth of a normal fault system: Observations from the Lake Malawi basin of the east African rift, J. Struct. Geol., 22(2), 159–168, doi:10.1016/S0191-8141(99)00157-1, 2000.

805 Cornell, C. A.: Engineering seismic risk analysis, Bull. Seismol. Soc. Am., 58(5), 1583–1606, doi:http://dx.doi.org/10.1016/0167-6105(83)90143-5, 1968.

Cowie, P. A. and Roberts, G. P.: Constraining slip rates and spacings for active normal faults, J. Struct. Geol., 23(12), 1901–1915, doi:10.1016/S0191-8141(01)00036-0, 2001.

Cowie, P. A., Roberts, G. P., Bull, J. M. and Visini, F.: Relationships between fault geometry, slip rate variability and

810 earthquake recurrence in extensional settings, Geophys. J. Int., 189(1), 143–160, doi:10.1111/j.1365-246X.2012.05378.x, 2012.

Cox, S. C., Stirling, M. W., Herman, F., Gerstenberger, M. and Ristau, J.: Potentially active faults in the rapidly eroding landscape adjacent to the Alpine Fault, central Southern Alps, New Zealand, Tectonics, 31(2), doi:10.1029/2011TC003038, 2012.

815 Craig, T. J. and Jackson, J. A.: Variations in the Seismogenic Thickness of East Africa, J. Geophys. Res. Solid Earth, 126(3), 1–15, doi:10.1029/2020JB020754, 2021.

Cramer, C. H., Petersen, M. D. and Reichle, M. S.: A Monte Carlo approach in estimating uncertainty for a seismic hazard assessment of Los Angeles, Ventura, and Orange Counties, California, Bull. Seismol. Soc. Am., 86(6), 1681–1691, 1996.

Das, S. and Scholz, C. H.: Why large earthquakes do not nucleate at shallow depths, Nature, 305(5935), 621–623, 1983.

820 Dawson, S. M., Laó-Dávila, D. A., Atekwana, E. A. and Abdelsalam, M. G.: The influence of the Precambrian Mughese Shear Zone structures on strain accommodation in the northern Malawi Rift, Tectonophysics, 722, 53–68, doi:10.1016/j.tecto.2017.10.010, 2018.

Delvaux, D. and Barth, A.: African stress pattern from formal inversion of focal mechanism data, Tectonophysics, 482(1–4), 105–128, doi:10.1016/j.tecto.2009.05.009, 2010.

825 Delvaux, D., Mulumba, J. L., Sebagenzi, M. N. S., Bondo, S. F., Kervyn, F. and Havenith, H. B.: Seismic hazard assessment of the Kivu rift segment based on a new seismotectonic zonation model (western branch, East African Rift system), J. African Earth Sci., 134, 831–855, doi:10.1016/j.jafrearsci.2016.10.004, 2017.

Dolan, J. F. and Meade, B. J.: A Comparison of Geodetic and Geologic Rates Prior to Large Strike-Slip Earthquakes: A Diversity of Earthquake-Cycle Behaviors?, Geochemistry, Geophys. Geosystems, 18(12), 4426–4436, doi:10.1002/2017GC007014, 2017.

830

DuRoss, C. B., Personius, S. F., Crone, A. J., Olig, S. S., Hylland, M. D., Lund, W. R. and Schwartz, D. P.: Fault segmentation: New concepts from the Wasatch Fault Zone, Utah, USA, J. Geophys. Res. Solid Earth, 121(2), 1131–1157, doi:10.1002/2015JB012519, 2016.

DuRoss, C. B., Gold, R. D., Briggs, R. W., Delano, J. E., Ostenaa, D. A., Zellman, M. S., Cholewinski, N., Wittke, S. J. and

835 Mahan, S. A.: Holocene earthquake history and slip rate of the southern Teton fault, Wyoming, USA, Bull. Geol. Soc. Am., 132(7–8), 1566–1586, doi:10.1130/B35363.1, 2020.

Ebinger, C. J.: Tectonic development of the western branch of the East African rift system, Geol. Soc. Am. Bull., 101(7), 885–903, doi:10.1130/0016-7606(1989)101<0885:TDOTWB>2.3.CO;2, 1989.

Ebinger, C. J., Oliva, S. J., Pham, T. Q., Peterson, K., Chindandali, P., Illsley-Kemp, F., Drooff, C., Shillington, D. J., Accardo,

840 N. J., Gallacher, R. J., Gaherty, J., Nyblade, A. A. and Mulibo, G.: Kinematics of Active Deformation in the Malawi Rift and Rungwe Volcanic Province, Africa, Geochemistry, Geophys. Geosystems, 20(8), 3928–3951, doi:10.1029/2019GC008354, 2019.

Fagereng, Å.: Fault segmentation, deep rift earthquakes and crustal rheology: Insights from the 2009 Karonga sequence and seismicity in the Rukwa-Malawi rift zone, Tectonophysics, 601, 216–225, doi:10.1016/j.tecto.2013.05.012, 2013.

845 Fagereng, Å. and Biggs, J.: New perspectives on 'geological strain rates'' calculated from both naturally deformed and actively deforming rocks,' J. Struct. Geol., 125, 100–110, doi:10.1016/j.jsg.2018.10.004, 2019.

Faleide, T. S., Braathen, A., Lecomte, I., Mulrooney, M. J., Midtkandal, I., Bugge, A. J. and Planke, S.: Impacts of seismic resolution on fault interpretation: Insights from seismic modelling, Tectonophysics, 816, 229008, doi:10.1016/j.tecto.2021.229008, 2021.

850 Faure Walker, J., Boncio, P., Pace, B., Roberts, G., Benedetti, L., Scotti, O., Visini, F. and Peruzza, L.: Fault2SHA Central Apennines database and structuring active fault data for seismic hazard assessment, Sci. Data, 8(1), 1–20, doi:10.1038/s41597-021-00868-0, 2021.

Fenton, C. H. and Bommer, J. J.: The Mw7 Machaze, Mozambique, earthquake of 23 February 2006, Seismol. Res. Lett., 77(4), 426–439, doi:10.1785/gssrl.77.4.426, 2006.

855 Field, E. H., Arrowsmith, R. J., Biasi, G. P., Bird, P., Dawson, T. E., Felzer, K. R., Jackson, D. D., Johnson, K. M., Jordan, T. H., Madden, C., Michael, A. J., Milner, K. R., Page, M. T., Parsons, T., Powers, P. M., Shaw, B. E., Thatcher, W. R., Weldon, R. J. and Zeng, Y.: Uniform California Earthquake Rupture Forecast, version 3 (UCERF3) -The time-independent model, Bull. Seismol. Soc. Am., 104(3), 1122–1180, doi:10.1785/0120130164, 2014.

Flannery, J. W. and Rosendahl, B. R.: The seismic stratigraphy of Lake Malawi, Africa: implications for interpreting geological

860 processes in lacustrine rifts, J. African Earth Sci., 10(3), 519–548, doi:10.1016/0899-5362(90)90104-M, 1990.

Fletcher, J. M., Teran, O. J., Rockwell, T. K., Oskin, M. E., Hudnut, K. W., Mueller, K. J., Spelz, R. M., Akciz, S. O., Masana,

E., Faneros, G., Fielding, E. J., Leprince, S., Morelan, A. E., Stock, J., Lynch, D. K., Elliott, A. J., Gold, P., Liu-Zeng, J., González-Ortega, A., Hinojosa-Corona, A. and González-García, J.: Assembly of a large earthquake from a complex fault system: Surface rupture kinematics of the 4 April 2010 El Mayor-Cucapah (Mexico) M w 7.2 earthquake, Geosphere, 10(4), 797–827, doi:10.1130/GES00933.1, 2014.

Gaherty, J. B., Zheng, W., Shillington, D. J., Pritchard, M. E., Henderson, S. T., Chindandali, P. R. N., Mdala, H., Shuler, A., Lindsey, N., Oliva, S. J., Nooner, S., Scholz, C. A., Schaff, D., Ekström, G. and Nettles, M.: Faulting processes during early-stage rifting: Seismic and geodetic analysis of the 2009-2010 Northern Malawi earthquake sequence, Geophys. J. Int., 217(3), 1767–1782, doi:10.1093/gji/ggz119, 2019.

Geist, E. L. and Parsons, T.: Distribution of Earthquakes on a Branching Fault System Using Integer Programming and Greedy-Sequential Methods, Geochemistry, Geophys. Geosystems, 21(9), 1–22, doi:10.1029/2020GC008964, 2020.

Gerstenberger, M. C., Marzocchi, W., Allen, T., Pagani, M., Adams, J., Danciu, L., Field, E. H., Fujiwara, H., Luco, N., Ma, K. F., Meletti, C. and Petersen, M. D.: Probabilistic Seismic Hazard Analysis at Regional and National Scales: State of the Art and Future Challenges, Rev. Geophys., 58(2), e2019RG000653, doi:10.1029/2019RG000653, 2020.

Giordano, N., De Risi, R., Voyagaki, E., Kloukinas, P., Novelli, V., Kafodya, I., Ngoma, I., Goda, K. and Macdonald, J.: Seismic fragility models for typical non-engineered URM residential buildings in Malawi, in Structures, vol. 32, pp. 2266–2278, Elsevier., 2021.

Goda, K., Gibson, E. D., Smith, H. R., Biggs, J. and Hodge, M.: Seismic risk assessment of urban and rural settlements around lake malawi, Front. Built Environ., 2, doi:10.3389/fbuil.2016.00030, 2016.

Goda, K., Novelli, V., De Risi, R., Kloukinas, P., Giordano, N., Macdonald, J., Kafodya, I., Ngoma, I. and Voyagaki, E.: Scenario-based earthquake risk assessment for central-southern Malawi: The case of the Bilila-Mtakataka Fault, Int. J. Disaster Risk Reduct., 102655, doi:https://doi.org/10.1016/j.ijdrr.2021.102655, 2021.

Goitom, B., Werner, M. J., Goda, K., Kendall, J. M., Hammond, J. O. S., Ogubazghi, G., Oppenheimer, C., Helmstetter, A., Keir, D. and Illsley-Kemp, F.: Probabilistic seismic-hazard assessment for Eritrea, Bull. Seismol. Soc. Am., 107(3), 1478–1494, doi:10.1785/0120160210, 2017.

Gómez-Novell, O., García-Mayordomo, J., Ortuño, M., Masana, E. and Chartier, T.: Fault System-Based Probabilistic Seismic Hazard Assessment of a Moderate Seismicity Region: The Eastern Betics Shear Zone (SE Spain), Front. Earth Sci., 8(December), doi:10.3389/feart.2020.579398, 2020.

Gupta, H. K. and Malomo, S.: The Malawi earthquake of March 10, 1989: A report of the macroseismic survey, Seismol. Res. Lett., 66(1), 20–27, doi:10.1016/0040-1951(92)90018-2, 1995.

Gupta, S., Cowie, P. A., Dawers, N. H. and Underhill, J. R.: A mechanism to explain rift-basin subsidence and stratigraphic patterns through fault-array evolution, Geology, 26(7), 595–598, doi:10.1130/0091-7613(1998)026<0595:AMTERB>2.3.CO, 1998.

Habgood, F.: The geology of the country west of the Shire River between Chikwawa and Chiromo, Bull. Geol. Surv. Malawi, 14, 1963.

Habgood, F., Holt, D. N. and Walshaw, R. D.: The geology of the Thyolo Area, Bull. Geol. Surv. Malawi, 22, 1973.

Hamiel, Y., Baer, G., Kalindekafe, L., Dombola, K. and Chindandali, P.: Seismic and aseismic slip evolution and deformation associated with the 2009-2010 northern Malawi earthquake swarm, East African Rift, Geophys. J. Int., 191(3), 898–908, doi:10.1111/j.1365-246X.2012.05673.x, 2012.

900   Hanks, T. C. and Bakun, W. H.: A bilinear source-scaling model for M-log a observations of continental earthquakes, Bull. Seismol. Soc. Am., 92(5), 1841–1846, doi:10.1785/0120010148, 2002.

Hellebrekers, N., Niemeijer, A. R., Fagereng, Å., Manda, B. and Mvula, R. L. S.: Lower crustal earthquakes in the East African Rift System: Insights from frictional properties of rock samples from the Malawi rift, Tectonophysics, 767, 228167, doi:10.1016/j.tecto.2019.228167, 2019.

905   Helmstetter, A. and Werner, M. J.: Adaptive spatiotemporal smoothing of seismicity for long-term earthquake forecasts in California, Bull. Seismol. Soc. Am., 102(6), 2518–2529, doi:10.1785/0120120062, 2012.

Henry, C. and Das, S.: Aftershock zones of large shallow earthquakes: Fault dimensions, aftershock area expansion and scaling relations, Geophys. J. Int., 147(2), 272–293, doi:10.1046/j.1365-246X.2001.00522.x, 2001.

Hetland, E. A. and Hager, B. H.: Interseismic strain accumulation: Spin-up, cycle invariance, and irregular rupture sequences,
910   Geochemistry, Geophys. Geosystems, 7(5), doi:10.1029/2005GC001087, 2006.

Hodge, M., Biggs, J., Goda, K. and Aspinall, W.: Assessing infrequent large earthquakes using geomorphology and geodesy: the Malawi Rift, Nat. Hazards, 76(3), 1781–1806, doi:10.1007/s11069-014-1572-y, 2015.

Hodge, M., Fagereng, A., Biggs, J. and Mdala, H.: Controls on Early-Rift Geometry: New Perspectives From the Bilila-Mtakataka Fault, Malawi, Geophys. Res. Lett., 45(9), 3896–3905, doi:10.1029/2018GL077343, 2018a.

915   Hodge, M., Fagereng, A. and Biggs, J.: The Role of Coseismic Coulomb Stress Changes in Shaping the Hard Link Between Normal Fault Segments, J. Geophys. Res. Solid Earth, 123(1), 797–814, doi:10.1002/2017JB014927, 2018b.

Hodge, M., Biggs, J., Fagereng, A., Elliott, A., Mdala, H. and Mphepo, F.: A semi-automated algorithm to quantify scarp morphology (SPARTA): Application to normal faults in southern Malawi, Solid Earth, 10(1), 27–57, doi:10.5194/se-10-27-2019, 2019.

920   Hodge, M., Biggs, J., Fagereng, Å., Mdala, H., Wedmore, L. N. . and Williams, J. N.: Evidence From High-Resolution Topography for Multiple Earthquakes on High Slip-to-Length Fault Scarps: The Bilila-Mtakataka Fault, Malawi, Tectonics, 39(2), e2019TC005933, doi:10.1029/2019TC005933, 2020.

Hopper, E., Gaherty, J. B., Shillington, D. J., Accardo, N. J., Nyblade, A. A., Holtzman, B. K., Havlin, C., Scholz, C. A., Chindandali, P. R. N., Ferdinand, R. W., Mulibo, G. D. and Mbogoni, G.: Preferential localized thinning of lithospheric mantle
925   in the melt-poor Malawi Rift, Nat. Geosci., 13(8), 584–589, doi:10.1038/s41561-020-0609-y, 2020.

Inman, H. F. and Bradley Jr, E. L.: The overlapping coefficient as a measure of agreement between probability distributions and point estimation of the overlap of two normal densities, Commun. Stat. Methods, 18(10), 3851–3874, 1989.

Jackson, J. and Blenkinsop, T.: The Malaŵi Earthquake of March 10, 1989: Deep faulting within the East African Rift System, Tectonics, 12(5), 1131–1139, doi:10.1029/93TC01064, 1993.

930 Jackson, J. and Blenkinsop, T.: The Bilila-Mtakataka fault in Malawi: an active, 100-km long, normal fault segment in thick seismogenic crust, Tectonics, 16(1), 137–150, doi:10.1029/96TC02494, 1997.

Kagan, Y. Y., Jackson, D. D. and Geller, R. J.: Characteristic earthquake model, 1884-2011, R.I.P., Seismol. Res. Lett., 83(6), 951–953, doi:10.1785/0220120107, 2012.

Kanamori, H. and Anderson, D. L.: Theoretical basis of some empirical relations in seismology, Bull. Seismol. Soc. Am.,

935 65(5), 1073–1095, 1975.

Kervyn, F., Ayub, S., Kajara, R., Kanza, E. and Temu, B.: Evidence of recent faulting in the Rukwa rift (West Tanzania) based on radar interferometric DEMs, J. African Earth Sci., 44(2), 151–168, doi:10.1016/j.jafrearsci.2005.10.008, 2006.

King, G. C. P.: Speculations on the geometry of the initiation and termination processes of earthquake rupture and its relation to morphology and geological structure, Pure Appl. Geophys. PAGEOPH, 124(3), 567–585, doi:10.1007/BF00877216, 1986.

940 Kolawole, F., Atekwana, E. A., Laó-Dávila, D. A., Abdelsalam, M. G., Chindandali, P. R., Salima, J. and Kalindekafe, L.: Active Deformation of Malawi Rift's North Basin Hinge Zone Modulated by Reactivation of Preexisting Precambrian Shear Zone Fabric, Tectonics, 37(3), 683–704, doi:10.1002/2017TC004628, 2018a.

Kolawole, F., Atekwana, E. A., Laó-Dávila, D. A., Abdelsalam, M. G., Chindandali, P. R., Salima, J. and Kalindekafe, L.: High-resolution electrical resistivity and aeromagnetic imaging reveal the causative fault of the 2009 Mw 6.0 Karonga, Malawi

945 earthquake, Geophys. J. Int., 213(2), 1412–1425, doi:10.1093/gji/ggy066, 2018b.

Kolawole, F., Firkins, M. C., Al Wahaibi, T. S., Atekwana, E. A. and Soreghan, M. J.: Rift interaction zones and the stages of rift linkage in active segmented continental rift systems, Basin Res., doi:10.1111/bre.12592, 2021a.

Kolawole, F., Phillips, T. B., Atekwana, E. A. and Jackson, C. A. L.: Structural Inheritance Controls Strain Distribution During Early Continental Rifting, Rukwa Rift, Front. Earth Sci., 9(August), 1–14, doi:10.3389/feart.2021.707869, 2021b.

950 Kolawole, F., Vick, T., Atekwana, E. A., Laó-Dávila, D. A., Costa, A. and Carpenter, B. M.: Strain Localization and Migration During the Pulsed Lateral Propagation of the Shire Rift Zone, East Africa, 2022.

Laõ-Dávila, D. A., Al-Salmi, H. S., Abdelsalam, M. G. and Atekwana, E. A.: Hierarchical segmentation of the Malawi Rift: The influence of inherited lithospheric heterogeneity and kinematics in the evolution of continental rifts, Tectonics, 34(12), 2399–2417, doi:10.1002/2015TC003953, 2015.

955 Leonard, M.: Earthquake fault scaling: Self-consistent relating of rupture length, width, average displacement, and moment release, Bull. Seismol. Soc. Am., 100(5 A), 1971–1988, doi:10.1785/0120090189, 2010.

Litchfield, N. J., Van Dissen, R., Sutherland, R., Barnes, P. M., Cox, S. C., Norris, R., Beavan, R. J., Langridge, R., Villamor, P., Berryman, K., Stirling, M., Nicol, A., Nodder, S., Lamarche, G., Barrell, D. J. A., Pettinga, J. R., Little, T., Pondard, N., Mountjoy, J. J. and Clark, K.: A model of active faulting in New Zealand, New Zeal. J. Geol. Geophys., 57(1), 32–56,

960 doi:10.1080/00288306.2013.854256, 2014.

Litchfield, N. J., Villamor, P., van Dissen, R. J., Nicol, A., Barnes, P. M., Barrell, D. J. A., Pettinga, J. R., Langridge, R. M., Little, T. A., Mountjoy, J. J., Ries, W. F., Rowland, J., Fenton, C., Stirling, M. W., Kearse, J., Berryman, K. R., Cochran, U. A., Clark, K. J., Hemphill-Haley, M., Khajavi, N., Jones, K. E., Archibald, G., Upton, P., Asher, C., Benson, A., Cox, S. C.,

Gasston, C., Hale, D., Hall, B., Hatem, A. E., Heron, D. W., Howarth, J., Kane, T. J., Lamarche, G., Lawson, S., Lukovic, B.,
McColl, S. T., Madugo, C., Manousakis, J., Noble, D., Pedley, K., Sauer, K., Stahl, T., Strong, D. T., Townsend, D. B., Toy, V., Williams, J., Woelz, S. and Zinke, R.: Surface rupture of multiple crustal faults in the 2016 Mw 7.8 Kaikōura, New Zealand, earthquake, Bull. Seismol. Soc. Am., 108(3B), 1496–1520, doi:10.1785/0120170300, 2018.

Macheyeki, A. S., Mdala, H., Chapola, L. S., Manhiça, V. J., Chisambi, J., Feitio, P., Ayele, A., Barongo, J., Ferdinand, R. W., Ogubazghi, G., Goitom, B., Hlatywayo, J. D., Kianji, G. K., Marobhe, I., Mulowezi, A., Mutamina, D., Mwano, J. M., Shumba, B. and Tumwikirize, I.: Active fault mapping in Karonga-Malawi after the December 19, 2009 Ms 6.2 seismic event, J. African Earth Sci., 102, 233–246, doi:10.1016/j.jafrearsci.2014.10.010, 2015.

Marzocchi, W., Taroni, M. and Selva, J.: Accounting for epistemic uncertainty in PSHA: Logic tree and ensemble modeling, Bull. Seismol. Soc. Am., 105(4), 2151–2159, doi:10.1785/0120140131, 2015.

McCalpin, J. P.: Paleoseismology, Academic press., 2009.

McGuire, R. K.: Probabilistic seismic hazard analysis and design earthquakes: closing the loop, Bull. - Seismol. Soc. Am., 85(5), 1275–1284, doi:10.1016/0148-9062(96)83355-9, 1995.

Middleton, T. A., Walker, R. T., Parsons, B., Lei, Q., Zhou, Y. and Ren, Z.: A major, intraplate, normal-faulting earthquake: The 1739 Yinchuan event in northern China, J. Geophys. Res. Solid Earth, 121(1), 293–320, doi:10.1002/2015JB012355, 2016.

Mildon, Z. K., Toda, S., Faure Walker, J. P. and Roberts, G. P.: Evaluating models of Coulomb stress transfer: Is variable fault geometry important?, Geophys. Res. Lett., 43(24), 12,407-412,414, doi:10.1002/2016GL071128, 2016.

Molnar, P.: Earthquake recurrence intervals and plate tectonics, Bull. Seismol. Soc. Am., 69(1), 115–133, 1979.

Morell, K. D., Styron, R., Stirling, M., Griffin, J., Archuleta, R. and Onur, T.: Seismic Hazard Analyses From Geologic and Geomorphic Data: Current and Future Challenges, Tectonics, 39(10), e2018TC005365, doi:10.1029/2018TC005365, 2020.

Mortimer, E. J., Paton, D. A., Scholz, C. A. and Strecker, M. R.: Implications of structural inheritance in oblique rift zones for basin compartmentalization: Nkhata Basin, Malawi Rift (EARS), Mar. Pet. Geol., 72, 110–121, doi:10.1016/j.marpetgeo.2015.12.018, 2016.

Muirhead, J. D., Kattenhorn, S. A., Lee, H., Mana, S., Turrin, B. D., Fischer, T. P., Kianji, G., Dindi, E. and Stamps, D. S.: Evolution of upper crustal faulting assisted by magmatic volatile release during early-stage continental rift development in the East African Rift, Geosphere, 12(6), 1670–1700, doi:10.1130/GES01375.1, 2016.

Muirhead, J. D., Wright, L. J. M. and Scholz, C. A.: Rift evolution in regions of low magma input in East Africa, Earth Planet. Sci. Lett., 506, 332–346, doi:10.1016/j.epsl.2018.11.004, 2019.

Neely, J. S. and Stein, S.: Why do continental normal fault earthquakes have smaller maximum magnitudes?, Tectonophysics, 809(November 2020), 228854, doi:10.1016/j.tecto.2021.228854, 2021.

Ngoma, I., Kafodya, I., Kloukinas, P., Novelli, V., Macdonald, J. and Goda, K.: Building classification and seismic vulnerability of current housing construction in Malawi, Malawi J. Sci. Technol., 11(1), 57–72, 2019.

Nicol, A., Van Dissen, R. J., Stirling, M. W. and Gerstenberger, M. C.: Completeness of the Paleoseismic Active-Fault Record

in New Zealand, Seismol. Res. Lett., 87(6), 1299–1310, doi:10.1785/0220160088, 2016.

Njinju, E. A., Kolawole, F., Atekwana, E. A. E. A., Stamps, D. S., Atekwana, E. A. E. A., Abdelsalam, M. G. and Mickus, K. L.: Terrestrial heat flow in the Malawi Rifted Zone, East Africa: Implications for tectono-thermal inheritance in continental rift basins, J. Volcanol. Geotherm. Res., 387, doi:10.1016/j.jvolgeores.2019.07.023, 2019.

Novelli, V., Kloukinas, P., De Risi, R., Kafodya, I., Ngoma, I., Macdonald, J. and Goda, K.: Seismic Mitigation Framework for Non-engineered Masonry Buildings in Developing Countries: Application to Malawi in the East African Rift, in Resilient Structures and Infrastructure, pp. 195–223, Springer., 2019.

Nyblade, A. A. and Langston, C. A.: East African earthquakes below 20 km depth and their implications for crustal structure, Geophys. J. Int., 121(1), 49–62, doi:10.1111/j.1365-246X.1995.tb03510.x, 1995.

Ojo, O., Thomson, S. N. and Lao-Davila, D.: Neogene - Quaternary Rifting of the Southern Malawi Rift and Linkage To the Late Carboniferous – Early Jurassic Shire Rift, Earth Sp. Sci. Open Arch. ESSOAr, (May), 1–58, doi:https://doi.org/10.1002/essoar.10511357.1, 2022a.

Ojo, O. O., Ohenhen, L. O., Kolawole, F., Johnson, S. G., Chindandali, P. R., Atekwana, E. A. and Laó-Dávila, D. A.: Under-Displaced Normal Faults: Strain Accommodation Along an Early-Stage Rift-Bounding Fault in the Southern Malawi Rift, Front. Earth Sci., 10, 1–19, doi:10.3389/feart.2022.846389, 2022b.

Olive, J. A., Behn, M. D. and Malatesta, L. C.: Modes of extensional faulting controlled by surface processes, Geophys. Res. Lett., 41(19), 6725–6733, doi:10.1002/2014GL061507, 2014.

Pace, B., Visini, F. and Peruzza, L.: FiSH : MATLAB Tools to Turn Fault Data into Seismic-Hazard Models, Seismol. Res. Lett., 87(2A), 374–386, doi:10.1785/0220150189, 2016.

Pagani, M., Monelli, D., Weatherill, G., Danciu, L., Crowley, H., Silva, V., Henshaw, P., Butler, L., Nastasi, M., Panzeri, L., Simionato, M. and Vigano, D.: Openquake engine: An open hazard (and risk) software for the global earthquake model, Seismol. Res. Lett., 85(3), 692–702, doi:10.1785/0220130087, 2014.

Pagani, M., Garcia-Pelaez, J., Gee, R., Johnson, K., Poggi, V., Silva, V., Simionato, M., Styron, R., Viganò, D., Danciu, L., Monelli, D. and Weatherill, G.: The 2018 version of the Global Earthquake Model: Hazard component, Earthq. Spectra, 36(1), 226–251, doi:10.1177/8755293020931866, 2020.

Peacock, D. C. P., Nixon, C. W., Rotevatn, A., Sanderson, D. J. and Zuluaga, L. F.: Glossary of fault and other fracture networks, J. Struct. Geol., 92, 12–29, doi:10.1016/j.jsg.2016.09.008, 2016.

Perea, H., Masana, E. and Santanach, P.: A pragmatic approach to seismic parameters in a region with low seismicity: The case of Eastern Iberia, Nat. Hazards, 39(3), 451–477, doi:10.1007/s11069-006-0013-y, 2006.

Petersen, M. D., Zeng, Y., Haller, K. M., McCaffrey, R., Hammond, W. C., Bird, P., Moschetti, M., Shen, Z., Bormann, J. and Thatcher, W.: Geodesy- and geology-based slip-rate models for the Western United States (excluding California) national seismic hazard maps, U.S. Geol. Surv. Open-File Rep. 2013-1293, 86, doi:10.3133/ofr20131293, 2014.

Petit, C. and Ebinger, C.: Flexure and mechanical behavior of cratonic lithosphere: Gravity models of the East African and Baikal rifts, J. Geophys. Res. Solid Earth, doi:10.1029/2000JB900101, 2000.

Plesch, A., Shaw, J. H., Benson, C., Bryant, W. A., Carena, S., Cooke, M., Dolan, J., Fuis, G., Gath, E., Grant, L., Hauksson, E., Jordan, T., Kamerling, M., Legg, M., Lindvall, S., Magistrale, H., Nicholson, C., Niemi, N., Oskin, M., Perry, S., Planansky, G., Rockwell, T., Shearer, P., Sorlien, C., Süss, M. P., Suppe, J., Treiman, J. and Yeats, R.: Community Fault Model (CFM) for southern California, Bull. Seismol. Soc. Am., 97(6), 1793–1802, doi:10.1785/0120050211, 2007.

Poggi, V., Durrheim, R., Tuluka, G. M., Weatherill, G., Gee, R., Pagani, M., Nyblade, A. and Delvaux, D.: Assessing seismic hazard of the East African Rift: a pilot study from GEM and AfricaArray, Bull. Earthq. Eng., 15(11), 4499–4529, doi:10.1007/s10518-017-0152-4, 2017.

Polonia, A., Gasperini, L., Amorosi, A., Bonatti, E., Bortoluzzi, G., Çagatay, N., Capotondi, L., Cormier, M. H., Gorur, N., McHugh, C. and Seeber, L.: Holocene slip rate of the North Anatolian Fault beneath the Sea of Marmara, Earth Planet. Sci. Lett., 227(3–4), 411–426, doi:10.1016/j.epsl.2004.07.042, 2004.

Rhoades, D. A., Christophersen, A., Gerstenberger, M. C., Liukis, M., Silva, F., Marzocchi, W., Werner, M. J. and Jordan, T. H.: Highlights from the first ten years of the New Zealand earthquake forecast testing center, Seismol. Res. Lett., 89(4), 1229–1237, 2018.

Robertson, E. A. M., Biggs, J., Cashman, K. V, Floyd, M. A. and Vye-Brown, C.: Influence of regional tectonics and pre-existing structures on the formation of elliptical calderas in the Kenyan Rift, in Geological Society Special Publication, vol. 420, pp. 43–67., 2016.

Sandwell, D., Mellors, R., Tong, X., Wei, M. and Wessel, P.: Open radar interferometry software for mapping surface Deformation, Eos, Trans. Am. Geophys. Union, doi:10.1029/2011EO280002, 2011.

Saria, E., Calais, E., Altamimi, Z., Willis, P. and Farah, H.: A new velocity field for Africa from combined GPS and DORIS space geodetic Solutions: Contribution to the definition of the African reference frame (AFREF), J. Geophys. Res. Solid Earth, 118(4), 1677–1697, doi:10.1002/jgrb.50137, 2013.

Scholz, C. A., Johnson, T. C., Cohen, A. S., King, J. W., Peck, J. A., Overpeck, J. T., Talbot, M. R., Brown, E. T., Kalindekafe, L., Amoako, P. Y. O., Lyons, R. P., Shanahan, T. M., Castañeda, I. S., Heil, C. W., Forman, S. L., McHargue, L. R., Beuning, K. R., Gomez, J. and Pierson, J.: East African megadroughts between 135 and 75 thousand years ago and bearing on early-modern human origins, Proc. Natl. Acad. Sci. U. S. A., 104(42), 16416–16421, doi:10.1073/pnas.0703874104, 2007.

Scholz, C. A., Shillington, D. J., Wright, L. J. M., Accardo, N., Gaherty, J. B. and Chindandali, P.: Intrarift fault fabric, segmentation, and basin evolution of the Lake Malawi (Nyasa) Rift, East Africa, Geosphere, 16(5), 1293–1311, doi:10.1130/GES02228.1, 2020.

Scholz, C. H. and Contreras, J. C.: Mechanics of continental rift architecture, Geology, 26(11), 967–970, doi:10.1130/0091-7613(1998)026<0967:MOCRA>2.3.CO, 1998.

Schwanghart, W. and Scherler, D.: Short Communication: TopoToolbox 2 - MATLAB-based software for topographic analysis and modeling in Earth surface sciences, Earth Surf. Dyn., 2(1), 1–7, doi:10.5194/esurf-2-1-2014, 2014.

Seebeck, H., Van Dissen, R. J., Litchfield, N. J., Barnes, P. M., Nicol, A., Langridge, R. M., Barrell, D. J. A., Villamor, P., Ellis, S. M., Rattenbury, M. S., Bannister, S., Gerstenberger, M. C., Ghisetti, F., Sutherland, R., Fraser, J., Nodder, S. D.,

Stirling, M. W., Humphrey, J., Bland, K. J., Howell, A., Mountjoy, J. J., Moon, V., Stahl, T., Spinardi, F., Townsend, D. B., Clark, K. J., Hamling, I. J., Cox, S. C., de Lange, W., Wopereis, P., Johnston, M., Morgenstern, R., Coffey, G. L., Eccles, J. D., Little, T. A., Fry, B., Griffin, J., Mortimer, N., Alcaraz, S. A., Massiot, C., Rowland, J., Muirhead, J., Upton, P., Hirschberg, H. and Lee, J. M.: New Zealand Community Fault Model – version 1.0., , 97, doi:doi:10.21420/GA7S-BS61. 1, 2022.

1070 Shaw, B. E.: Earthquake surface slip-length data is fit by constant stress drop and is useful for seismic hazard analysis, Bull. Seismol. Soc. Am., 103(2 A), 876–893, doi:10.1785/0120110258, 2013.

Shaw, B. E. and Scholz, C. H.: Slip-length scaling in large earthquakes: Observations and theory and implications for earthquake physics, Geophys. Res. Lett., 28(15), 2995–2998, doi:10.1029/2000GL012762, 2001.

Shillington, D. J., Gaherty, J. B., Ebinger, C. J., Scholz, C. A., Selway, K., Nyblade, A. A., Bedrosian, P. A., Class, C., Nooner,
1075 S. L., Pritchard, M. E., Elliott, J., Chindandali, P. R. N., Mbogoni, G., Ferdinand, R. W., Boniface, N., Manya, S., Kamihanda, G., Saria, E., Mulibo, G., Salima, J., Mruma, A., Kalindekafe, L., Accardo, N. J., Ntambila, D., Kachingwe, M., Mesko, G. T., McCartney, T., Maquay, M., O'Donnell, J. P., Tepp, G., Mtelela, K., Trinhammer, P., Wood, D., Aaron, E., Gibaud, M., Rapa, M., Pfeifer, C., Mphepo, F., Gondwe, D., Arroyo, G., Eddy, C., Kamoga, B. and Moshi, M.: Acquisition of a unique onshore/offshore geophysical and geochemical dataset in the northern Malawi (Nyasa) rift, Seismol. Res. Lett., 87(6), 1406–
1080 1416, doi:10.1785/0220160112, 2016.

Shillington, D. J., Scholz, C. A., Chindandali, P. R. N., Gaherty, J. B., Accardo, N. J., Onyango, E., Ebinger, C. J. and Nyblade, A. A.: Controls on Rift Faulting in the North Basin of the Malawi (Nyasa) Rift, East Africa, Tectonics, 39(3), e2019TC005633, doi:10.1029/2019TC005633, 2020.

Shyu, J. B. H., Chuang, Y. R., Chen, Y. L., Lee, Y. R. and Cheng, C. T.: A new on-land seismogenic structure source database
1085 from the Taiwan earthquake model (TEM) project for seismic hazard analysis of Taiwan, Terr. Atmos. Ocean. Sci., 27(3), 311–323, doi:10.3319/TAO.2015.11.27.02(TEM), 2016.

Stevens, V. L., Sloan, R. A., Chindandali, P. R., Wedmore, L. N. J., Salomon, G. W. and Muir, R. A.: The Entire Crust can be Seismogenic: Evidence from Southern Malawi, Tectonics, 40(6), e2020TC006654, doi:10.1029/2020tc006654, 2021.

Stirling, M., McVerry, G., Gerstenberger, M., Litchfield, N., Van Dissen, R., Berryman, K., Barnes, P., Wallace, L., Villamor,
1090 P., Langridge, R., Lamarche, G., Nodder, S., Reyners, M., Bradley, B., Rhoades, D., Smith, W., Nicol, A., Pettinga, J., Clark, K. and Jacobs, K.: National seismic hazard model for New Zealand: 2010 update, Bull. Seismol. Soc. Am., 102(4), 1514–1542, doi:10.1785/0120110170, 2012.

Stirling, M., Goded, T., Berryman, K. and Litchfield, N.: Selection of earthquake scaling relationships for seismic-hazard analysis, Bull. Seismol. Soc. Am., 103(6), 2993–3011, doi:10.1785/0120130052, 2013.

1095 Strader, A., Schneider, M. and Schorlemmer, D.: Prospective and retrospective evaluation of five-year earthquake forecast models for California, Geophys. J. Int., 211(1), 239–251, 2017.

Styron, R. and Pagani, M.: The GEM Global Active Faults Database, Earthq. Spectra, 36(1_suppl), 160–180, doi:10.1177/8755293020944182, 2020.

Styron, R., García-Pelaez, J. and Pagani, M.: CCAF-DB: The Caribbean and Central American active fault database, Nat.

1100   Hazards Earth Syst. Sci., 20(3), 831–857, doi:10.5194/nhess-20-831-2020, 2020.

Sun, M., Gao, S. S., Liu, K. H., Mickus, K., Fu, X. and Yu, Y.: Receiver function investigation of crustal structure in the Malawi and Luangwa rift zones and adjacent areas, Gondwana Res., 89, 168–176, doi:10.1016/j.gr.2020.08.015, 2021.

Taroni, M., Marzocchi, W., Schorlemmer, D., Werner, M. J., Wiemer, S., Zechar, J. D., Heiniger, L. and Euchner, F.: Prospective CSEP evaluation of 1-day, 3-month, and 5-yr earthquake forecasts for Italy, Seismol. Res. Lett., 89(4), 1251–

1105   1261, 2018.

Thingbaijam, K. K. S., Mai, P. M. and Goda, K.: New empirical earthquake source-scaling laws, Bull. Seismol. Soc. Am., 107(5), 2225–2246, doi:10.1785/0120170017, 2017.

Turcotte, D. L. and Schubert, G.: Geodynamics: Applications of continuum physics to geological problems, 450 pp, 1982.

Valentini, A., DuRoss, C. B., Field, E. H., Gold, R. D., Briggs, R. W., Visini, F. and Pace, B.: Relaxing Segmentation on the

1110   Wasatch Fault Zone: Impact on Seismic Hazard, Bull. Seismol. Soc. Am., 110(1), 83–109, doi:10.1785/0120190088, 2020.

Vallage, A. and Bollinger, L.: Testing Fault Models in Intraplate Settings: A Potential for Challenging the Seismic Hazard Assessment Inputs and Hypothesis?, Pure Appl. Geophys., 177(5), 1879–1889, doi:10.1007/s00024-019-02129-z, 2020.

Visini, F., Valentini, A., Chartier, T., Scotti, O. and Pace, B.: Computational Tools for Relaxing the Fault Segmentation in Probabilistic Seismic Hazard Modelling in Complex Fault Systems, Pure Appl. Geophys., 177(5), 1855–1877,

1115   doi:10.1007/s00024-019-02114-6, 2020.

Vittori, E., Delvaux, D. and Kervyn, F.: Kanda fault: A major seismogenic element west of the Rukwa Rift (Tanzania, East Africa), J. Geodyn., 24(1–4), 139–153, doi:10.1016/S0264-3707(96)00038-5, 1997.

Wallace, L. M., Barnes, P., Beavan, J., Van Dissen, R., Litchfield, N., Mountjoy, J., Langridge, R., Lamarche, G. and Pondard, N.: The kinematics of a transition from subduction to strike-slip: An example from the central New Zealand plate boundary,

1120   J. Geophys. Res. Solid Earth, 117(2), doi:10.1029/2011JB008640, 2012.

Wallace, R. E.: Earthquake recurrence intervals on the San Andreas fault, Bull. Geol. Soc. Am., 81(10), 2875–2890, doi:10.1130/0016-7606(1970)81[2875:ERIOTS]2.0.CO;2, 1970.

Walshaw, R. D.: The Geology of the Nchue-Balaka Area, Bull. Geol. Surv. Malawi, 19, 1965.

Walter, J.: The Geology of the Salima-Mvera Mission Area, Bull. Geol. Surv. Malawi, 30, 1972.

1125   Walters, R. J., Gregory, L. C., Wedmore, L. N. J., Craig, T. J., McCaffrey, K., Wilkinson, M., Chen, J., Li, Z., Elliott, J. R., Goodall, H., Iezzi, F., Livio, F., Michetti, A. M., Roberts, G. and Vittori, E.: Dual control of fault intersections on stop-start rupture in the 2016 Central Italy seismic sequence, Earth Planet. Sci. Lett., 500, 1–14, doi:10.1016/j.epsl.2018.07.043, 2018.

Wang, T., Feng, J., Liu, K. H. and Gao, S. S.: Crustal structure beneath the Malawi and Luangwa Rift Zones and adjacent areas from ambient noise tomography, Gondwana Res., 67, 187–198, doi:10.1016/j.gr.2018.10.018, 2019.

1130   Wedmore, L. N. J., Faure Walker, J. P., Roberts, G. P., Sammonds, P. R., McCaffrey, K. J. W. and Cowie, P. A.: A 667 year record of coseismic and interseismic Coulomb stress changes in central Italy reveals the role of fault interaction in controlling irregular earthquake recurrence intervals, J. Geophys. Res. Solid Earth, 122(7), 5691–5711, doi:10.1002/2017JB014054, 2017.

Wedmore, L. N. J., Biggs, J., Williams, J. N., Fagereng, Å., Dulanya, Z., Mphepo, F. and Mdala, H.: Active Fault Scarps in

Southern Malawi and Their Implications for the Distribution of Strain in Incipient Continental Rifts, Tectonics, 39(3), e2019TC005834, doi:10.1029/2019TC005834, 2020a.

Wedmore, L. N. J., Williams, J. N., Biggs, J., Fagereng, Å., Mphepo, F., Dulanya, Z., Willoughby, J., Mdala, H. and Adams, B. A.: Structural inheritance and border fault reactivation during active early-stage rifting along the Thyolo fault, Malawi, J. Struct. Geol., 139, 104097, doi:10.1016/j.jsg.2020.104097, 2020b.

Wedmore, L. N. J., Biggs, J., Floyd, M., Fagereng, Mdala, H., Chindandali, P., Williams, J. N. and Mphepo, F.: Geodetic Constraints on Cratonic Microplates and Broad Strain During Rifting of Thick Southern African Lithosphere, Geophys. Res. Lett., 48(17), doi:10.1029/2021GL093785, 2021.

Weldon, R., Scharer, K., Fumal, T. and Biasi, G.: Wrightwood and the earthquake cycle: What a long recurrence record tells us about how faults work, GSA Today, 14(9), 4–10, doi:10.1130/1052-5173(2004)014<4:WATECW>2.0CO;2, 2004.

Wells, D. L. and Coppersmith, K. J.: New Empirical Relationships among Magnitude, Rupture Length, Rupture Width, Rupture Area, and Surface Displacement, Bull. Seismol. Soc. Am., 84(4), 974–1002, doi:<p></p>, 1994.

Wesnousky, S. G.: Displacement and geometrical characteristics of earthquake surface ruptures: Issues and implications for seismic-hazard analysis and the process of earthquake rupture, Bull. Seismol. Soc. Am., 98(4), 1609–1632, doi:10.1785/0120070111, 2008.

Wheeler, W. H. and Rosendahl, B. R.: Geometry of the Livingstone Mountains Border Fault, Nyasa (Malawi) Rift, East Africa, Tectonics, 13(2), 303–312, doi:10.1029/93TC02314, 1994.

Widess, M. B.: How Thin Is a Thin Bed?, Geophysics, 38(6), 1176–1180, doi:10.1190/1.1440403, 1973.

Williams, J., Werner, M., Goda, K., Wedmore, L., Risi, R. De, Biggs, J., Mdala, H., Dulanya, Z., Fagereng, Å., Mphepo, F. and Chindandali, P.: Fault-based Probabilistic Seismic Hazard Analysis in Regions with Low Strain Rates and a Thick Seismogenic Layer: A Case Study from Malawi, Nat. Hazards Prepr. (Version 1) available Res. Sq., doi:10.21203/rs.3.rs-1452299/v1, 2022a.

Williams, J. N., Fagereng, Å., Wedmore, L. N. J., Biggs, J., Mphepo, F., Dulanya, Z., Mdala, H. and Blenkinsop, T.: How Do Variably Striking Faults Reactivate During Rifting? Insights From Southern Malawi, Geochemistry, Geophys. Geosystems, 20(7), 3588–3607, doi:10.1029/2019GC008219, 2019.

Williams, J. N., Mdala, H., Fagereng, Å., Wedmore, L. N. J., Biggs, J., Dulanya, Z., Chindandali, P. and Mphepo, F.: A systems-based approach to parameterise seismic hazard in regions with little historical or instrumental seismicity: Active fault and seismogenic source databases for southern Malawi, Solid Earth, 12(1), 187–217, doi:10.5194/se-12-187-2021, 2021a.

Williams, J. N., Wedmore, L. N. J., Scholz, C. A., Kolawole, F., Wright, L. J. M., Shillington, D. J., Fagereng, Å., Biggs, J., Mdala, H., Dulanya, Z., Mphepo, F., Chindandali, P. and Werner, M. J.: Malawi Active Fault Database (v1.0) [Data set], , doi:10.5281/ZENODO.5507190, 2021b.

Williams, J. N., Wedmore, L. N. J., Scholz, C. A., Kolawole, F., Wright, L. J. M., Shillington, D. J., Fagereng, Å., Biggs, J., Mdala, H., Dulanya, Z., Mphepo, F., Chindandali, P. and Werner, M. J.: The Malawi Active Fault Database: an onshore-offshore database for regional assessment of seismic hazard and tectonic evolution, Geochemistry, Geophys. Geosystems,

23(5), e2022GC010425, doi:10.1029/2022gc010425, 2022b.

Wright, L. J. M., Muirhead, J. D. and Scholz, C. A.: Spatiotemporal Variations in Upper Crustal Extension Across the Different

1170   Basement Terranes of the Lake Tanganyika Rift, East Africa, Tectonics, 39(3), doi:10.1029/2019TC006019, 2020.

Xu, Y., He, H., Deng, Q., Allen, M. B., Sun, H. and Bi, L.: The CE 1303 Hongdong Earthquake and the Huoshan Piedmont Fault, Shanxi Graben: Implications for Magnitude Limits of Normal Fault Earthquakes, J. Geophys. Res. Solid Earth, 123(4), 3098–3121, doi:10.1002/2017JB014928, 2018.

Youngs, R. R. and Coppersmith, K. J.: Implications of fault slip rates and earthquake recurrence models to probabilistic seismic

1175   hazard estimates, Bull. Seismol. Soc. Am., 75(4), 939–964, 1985.

Zechar, J. D. and Frankel, K. L.: Incorporating and reporting uncertainties in fault slip rates, J. Geophys. Res. Solid Earth, 114(12), 1–9, doi:10.1029/2009JB006325, 2009.

Zechar, J. D., Schorlemmer, D., Werner, M. J., Gerstenberger, M. C., Rhoades, D. A. and Jordan, T. H.: Regional earthquake likelihood models I: First-order results, Bull. Seismol. Soc. Am., 103(2A), 787–798, 2013.

1180   Zeng, Y. and Shen, Z. K.: Fault network modeling of crustal deformation in California constrained using GPS and geologic observations, Tectonophysics, 612–613, 1–17, doi:10.1016/j.tecto.2013.11.030, 2014.

Zheng, W., Oliva, S. J., Ebinger, C. and Pritchard, M. E.: Aseismic Deformation During the 2014 Mw 5.2 Karonga Earthquake, Malawi, From Satellite Interferometry and Earthquake Source Mechanisms, Geophys. Res. Lett., 47(22), doi:10.1029/2020GL090930, 2020.

1185